INSTITUT FÜR INFORMATIK

UND PRAKTISCHE MATHEMATIK

**The Poisson Scale-Space:
A Unified Approach to Phase-Based
Image Processing in Scale-Space**

Michael Felsberg
Gerald Sommer

Bericht Nr. 0208
14. August 2002

PAX OPTIMA RERUM

CHRISTIAN-ALBRECHTS-UNIVERSITÄT

KIEL

The Poisson Scale-Space:
A Unified Approach to Phase-Based
Image Processing in Scale-Space

Michael Felsberg
Gerald Sommer

e-mail: mfe@isy.liu.se

Dieser Bericht ist als persönliche Mitteilung aufzufassen.

The Poisson Scale-Space:
A Unified Approach to Phase-Based Image Processing in Scale-Space

Michael Felsberg

Computer Vision Laboratory

Department of Electrical Engineering

Linköping University

SE-581 83 Linköping, Sweden

`mfe@isy.liu.se`

Gerald Sommer

Cognitive Systems Group

Institute of Computer Science

and Applied Mathematics

Christian-Albrechts-University of Kiel

D-24105 Kiel, Germany

`gs@ks.informatik.uni-kiel.de`

Abstract

In this paper we address the topics of scale-space and phase-based signal processing in a common framework. The involved linear scale-space is no longer based on the Gaussian kernel but on the Poisson kernel. The resulting scale-space representation is directly related to the monogenic signal, a 2D generalization of the analytic signal. Hence, the local phase arises as a natural concept in this framework which results in several advanced relationships that can be used in image processing.

Keywords: Poisson kernel, scale-space, phase-based image processing, monogenic signal

1 Introduction

Scale-space representation is a well established technique in image processing. Linear scale-space is commonly equated with the Gaussian kernel and the heat (diffusion) equation. Investigations on these two approaches have led to a huge number of refinements and algorithms which have proven to be sophisticated methods for various applications.

Phase-based signal processing is a powerful technique for the analysis of structure based on the approach of quadrature filters. Although quadrature filters make use of bandpass filters, and therefore they are related to scale-space, the theory of the analytic signal and the scale-space theory are unrelated and independent frameworks, yet.

1.1 Overview of the Paper

This paper addresses the topic of combining scale-space theory and phase-based signal processing. In order to obtain an appropriate common theoretic framework, a linear scale-space is introduced which is not based on the heat equation. We replace the Gaussian kernel with the Poisson kernel, which is related to the potential (Laplace) equation.

Adopting the idea of splitting the heat (diffusion) equation into the continuity equation and Fick's law [40], the image flux, or figure flow, is no longer given by the gradient of the scale-space representation, but by its generalized Hilbert transform. Combining the latter with with the scale-space representation yields a generalization of the analytic signal in scale-space. As a consequence, a powerful theoretic framework is derived, which can be used for various image processing tasks.

The paper is organized as follows. In Section 1.2 we give a brief overview on the axiomatic of linear scale-space.

In Section 2 we introduce the Poisson scale-space motivated by a simple geometric optical setting (Section 2.1) and verify if it fulfills the mentioned axiomatics (Section 2.2). In Section 2.3 we relate the Poisson kernel to the Laplace equation and derive certain relationships. The topic of causality is treated in Section 2.4 and by considering further properties of the Poisson scale-space (Section 2.5), we conclude the second part.

Section 3 deals with the combination of scale-space and phase-based image processing. We start with differential phase congruency as a method for edge detection (Section 3.1). After recalling several facts about the relationship between attenuation and phase in 1D (Section 3.2), we establish a similar theorem for the 2D case in Section 3.3. Using these results, we relate phase-based and amplitude-based image processing methods on a theoretic level (Section 3.4).

The paper is concluded with some final remarks, the appendix, and the references.

1.2 Axiomatics of Linear Scale-Space

In the scale-space literature, there are a couple of papers referring to the Gaussian scale-space as *the only linear scale-space*, e.g., [22, 1, 29]. According to [41] the axiomatic presented in [22] is the first attempt for the definition of a linear scale-space. The axiomatic is based on the assumption that there is an observation transformation Φ which transforms an image[1] $f(\mathbf{x})$ ($\mathbf{x} = (x, y)^T \in \mathbb{R}^2$) into a blurred version of the image $f_\Sigma(\mathbf{x})$. The observation transformation has the general form

$$f_\Sigma(\mathbf{x}) = \Phi(f(\mathbf{x}'), \mathbf{x}, \Sigma) = \int_{\mathbb{R}^2} \phi(f(\mathbf{x}'), \mathbf{x}, \mathbf{x}', \Sigma) \, d\mathbf{x}' \;, \tag{1}$$

where Σ is a 2×2 matrix. If the observation transformation fulfills certain constrains, it establishes a *linear scale-space*:

---

[1]Since we are interested in scale-space axiomatics for image processing, we only consider formulations for 2D signals. Note that we use the notion of 2D scale-space, although the scale-space representation is a 3D function.

Definition 1 (linear scale-space) *An observation transformation defines a linear scale-space if it fulfills the subsequent axioms:*

 A1. It is linear (wrt. multiplications).

 A2. It is shift invariant.

 A3. It fulfills the semigroup property.

 A4. It is scale invariant and closed under affine transformations.

 A5. It preserves positivity.

According to [41] (respectively [23]) we specify the axioms more formal:

 A1. means that $\Phi(\lambda f(\mathbf{x}'), \mathbf{x}, \Sigma) = \lambda \Phi(f(\mathbf{x}'), \mathbf{x}, \Sigma)$ for any $\lambda \in \mathbb{R}$.

 A2. means that $\Phi(f(\mathbf{x}' - \mathbf{s}), \mathbf{x}, \Sigma) = \Phi(f(\mathbf{x}'), \mathbf{x} - \mathbf{s}, \Sigma)$ for any $\mathbf{s} \in \mathbb{R}^2$.

 A3. means that there exists a mapping $S : \mathbb{R}^{2\times 2} \times \mathbb{R}^{2\times 2} \to \mathbb{R}^{2\times 2}$ so that
   $\Phi(\Phi(f(\mathbf{x}''), \mathbf{x}', \Sigma_1), \mathbf{x}, \Sigma_2) = \Phi(f(\mathbf{x}''), \mathbf{x}, S(\Sigma_1, \Sigma_2))$ for any Σ_1, Σ_2.

 A4. means that there exists a mapping $T : \mathbb{R}^{2\times 2} \times \mathbb{R}^{2\times 2} \to \mathbb{R}^{2\times 2}$ so that
   $\Phi(f(\mathbf{A}\mathbf{x}'), \mathbf{x}, \Sigma) = \Phi(f(\mathbf{x}'), \mathbf{A}\mathbf{x}, T(\Sigma, \mathbf{A}))$ for any $\mathbf{A} \in \mathrm{GL}(2)$.

 A5. means that $\Phi(f(\mathbf{x}'), \mathbf{x}, \Sigma) > 0$ for any $f > 0$ and for any positive definite Σ.

In case of *isotropic* or *rotation invariant* scale-space, the matrix Σ in the observation transformation (1) is replaced with a positive real number σ. The axiom A4 then boils down to

 A4'. It is scale and rotation invariant.

Scale and rotation invariance means that there exists a mapping $T : \mathbb{R} \times \mathbb{R} \to \mathbb{R}$ so that $\Phi(f(a\mathbf{R}\mathbf{x}'), \mathbf{x}, \sigma) = \Phi(f(\mathbf{x}'), a\mathbf{R}\mathbf{x}, T(\sigma, a))$ for any $a \in \mathbb{R}^+$ and any $\mathbf{R} \in \mathrm{SO}(2)$.
  Besides the axiomatic of Iijima, a couple of further axiomatics appeared in the literature. In this paper we only consider some additional axioms to those above; for a more exhaustive overview we refer to [41]. For each axiom we give either the original reference or the name of the author (the original reference can be found in [41]). The different axioms refer to either to the observation transformation (respectively the generating convolution kernel) or the *image flux*. The image flux, or *figure flow*, is the vector field whose divergence compensates the change of the signal through scale, i.e., the flux and the scale-space representation are related by the continuity equation [40].

 A6. The flux is given by the maximum loss of 'figure impression' (Iijima).

 A7. The kernel must be separable (Otsu).

A8. The scale-space must fulfill the causality requirement, i.e., isophotes must be connected to the original signal [25].

A9. Isophotes in scale-space must be upwards convex [25]; local maxima should not enhance with scale [1, 30].[2]

A10. No new maxima should be created with increasing scale (only valid in 1D [1]).

Based upon the mentioned axiomatics of linear scale-space, the convolution with a Gaussian kernel can be used to create blurred versions of the original image. In order to speed up the calculation, the blurred versions of the image are subsampled, yielding a resolution pyramid [18, 7]. Instead of performing convolutions, one can implement scale-space filtering using the underlying partial differential equation, in the Gaussian scale-space the heat equation. The advantage of this method is that it is also possible to implement a non-linear heat equation, i.e., having a shift variant operator. This leads to non-linear diffusion methods [34, 8]. A further enhancement is obtained by replacing the scalar-valued diffusivity with a tensor-valued diffusivity, yielding anisotropic diffusion methods [40, 39, 37]. However, all these refinements of linear scale-space are out of the scope of this paper. We rather focus on the linear case, showing that there is another linear scale-space which fulfills most of the mentioned axioms.

---

[2]We explicitly distinguish between the causality requirement (axiom A8) and the non-enhancement, since the informal definition of causality is slightly weaker than the convexity constrain (see Section 2.4).

2 Another Linear Scale-Space

In this section we introduce a new[3] linear scale-space, the *Poisson scale-space*. We motivate it by some considerations from geometric optics and by a projective mapping. Furthermore, we show that the Poisson scale-space fulfills some important axiomatics which have appeared in the literature so far and discuss its behavior concerning level crossings and local extrema.

2.1 Defocusing of an Optical System

The Gaussian scale-space is claimed to be related to the *defocusing of an idealized optical system* [41]. However, a careful consideration of the physical settings in an optical system does *not* necessarily result in Gaussian blurring but in an image convolved with the *Poisson kernel*. Consider the simple optical system in Fig. 1, showing a sketched object mapped
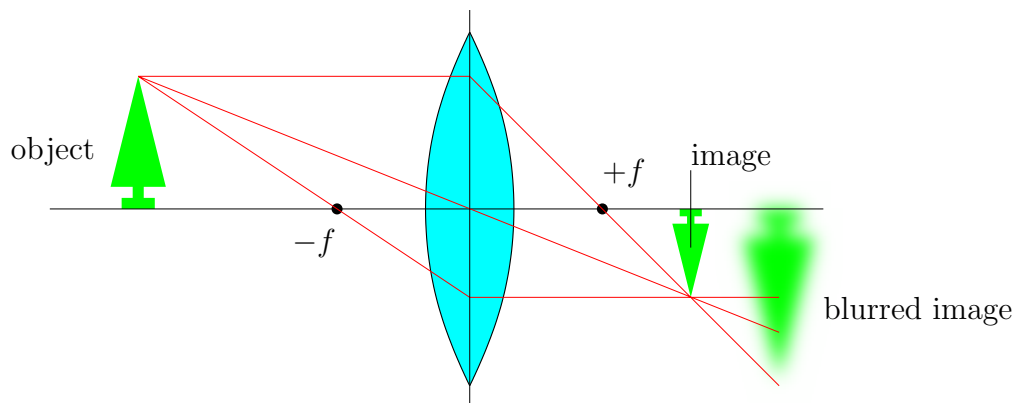

Figure 1: A simple optical system. The object (tree) is mapped through a thin lens with focal length f onto two image planes. The first (sharp) image is at the right distance of the lens, whereas the second one is blurred since it is at a too large distance, i.e., it is defocused.

through a thin lens onto two image planes. The first image is sharp, i.e., the system is focused, whereas the second one results from a defocused system, i.e., it is blurred. The further we move the image plane the more blurred the image looks like. By an appropriate rescaling of the image, this successive blurring corresponds to a descend through a scale-space. Hence, the blurring operator which acts on the image in the optical system can be considered to be the generating kernel of a scale-space. In our opinion, there is no reason

---

[3]Actually, the Poisson scale-space is not totally new: In [33] Pauwels et. al. have considered a class of scale-space kernels, among which they also mentioned explicitly the 1D Poisson kernel (Cauchy density). In our two conference papers [17, 16], the Poisson kernel already appeared in the context of scale-space, which was further discussed in [13]. Independently, Duits et. al. started investigations about scale-space axiomatics, first results can be found in [9, 10].

to choose another physical setting (e.g. heat conduction) than an optical for the physical motivation of scale-space in image processing.

In order to derive the operator from the physical setting, we make at first certain assumptions:

- The considered objects reflect the light into all directions in the same way.[4] This assumption implies that the surfaces of all objects are dull and do not have specular points.

- The lens is infinite large. Further below we explain what happens if the lens is finite.

- The object is flat and parallel to the lens, i.e., it has a constant depth. We comment on this below as well.

From the first assumption we conclude that the light intensity emitted from a certain point of the object is constant on any semi-sphere facing to the lens. Due to the third assumption, no occlusion can occur and on the full semi-sphere the intensity is constant for any radius. Hence, any light-ray emitted from that object point going through the unit semi-sphere eventually hits the lens. The intensity distribution on the lens is however not constant any more. Approximating the thin lens by a plane, the distribution is obtained from a gnomonic projection, see Fig. 2. In the gnomonic projection, a point on the semi-sphere
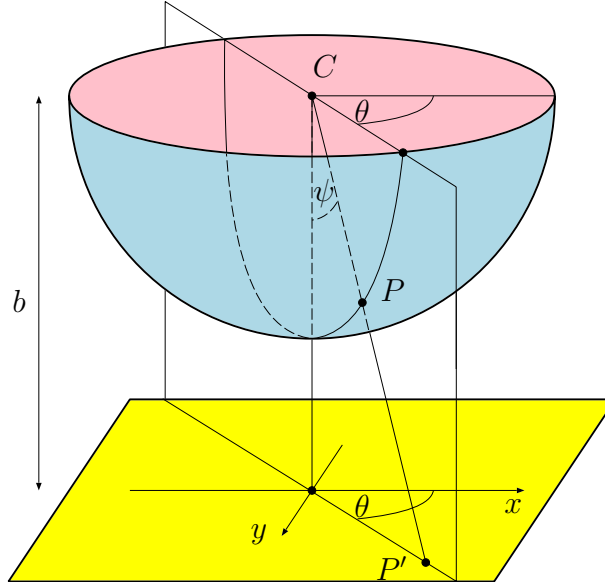

Figure 2: Gnomonic projection of a point P on the sphere onto the point P' on the plane. The distance of the sphere center C to the plane is indicated by b.

---

[4]At this point, we do not take into account the Lambertian law; we rather consider each object point as a point source, emerging light into all directions in the same way.

P is projected onto the point P' on the plane which is at a distance of b from the sphere center C. The point in the plane is given by the intersection of the plane and the line through C and P.

Returning to the constant intensity distribution on the unit semi-sphere, let us assume that the intensity is given by

$$I(\theta, \psi) = I_{\mathrm{t}}\, p(\theta, \psi) = I_{\mathrm{t}} \frac{\sin\psi\, d\psi\, d\theta}{2\pi} \tag{2}$$

so that the integral of $p(\theta, \psi)$ over the semi-sphere is one, i.e., $p(\theta, \psi)$ can be considered as a probability density function. Based on the geometry of the gnomonic projection, we want to compute the resulting intensity in the plane: $I'_b(\mathbf{x}) = I_{\mathrm{t}} p'_b(\mathbf{x})$. In a first step, we switch to polar coordinates by setting $x = r\cos\theta$ and $y = r\sin\theta$. Whereas the angular coordinate θ remains unchanged under the gnomonic projection, the relationship between ψ and r is given as

$$r = b\tan\psi \qquad \text{and} \qquad \psi = \arctan\left(\frac{r}{b}\right) \tag{3}$$

and hence,

$$d\psi = \left(1 + \frac{r^2}{b^2}\right)^{-1} \frac{1}{b}\, dr = \frac{b}{b^2 + r^2}\, dr\ . \tag{4}$$

Plugging the identities $\sin\psi = r/\sqrt{r^2 + b^2}$ and (4) into (2) yields

$$p(\theta, \psi) = \frac{\sin\psi\, d\psi\, d\theta}{2\pi} = \frac{r}{\sqrt{r^2 + b^2}} \frac{b}{2\pi(b^2 + r^2)}\, dr\, d\theta \tag{5}$$

and switching back to Cartesian coordinates ($r\, dr\, d\theta = d\mathbf{x}$) results in

$$p'_b(\mathbf{x}) = \frac{b}{2\pi(b^2 + x^2 + y^2)^{3/2}}\, d\mathbf{x}\ . \tag{6}$$

The density function $p'_b(\mathbf{x})$ is a two-dimensional generalization of the *Cauchy probability density function* [11]. The density function without the differentials yields the convolution kernel

$$p(\mathbf{x}; b) = \frac{b}{2\pi(b^2 + |\mathbf{x}|^2)^{3/2}} \tag{7}$$

which is known as the 2D *Poisson kernel* [38].

We thus know that the intensity distribution at the lens plane is given by the 2D Poisson kernel. Furthermore, the distribution in every plane parallel to the lens is also of this type, but with a different parameter b. For parallel planes closer to the object than the lens position, b decreases. Same for planes between the lens and the sharp image. If the plane tends to the position where the sharp image is located, b tends to zero and $p(\mathbf{x}; b)$ tends to a 2D Dirac delta function (see Lemma 1). If the image plane is moved beyond the sharp image, b increases again and the image appears blurred with $p(\mathbf{x}; b)$.

Lemma 1 *If b tends to zero, $p(\mathbf{x}; b)$ tends to a 2D Dirac delta function:*

$$\lim_{b \to 0} p(\mathbf{x}; b) = \delta_0(\mathbf{x}) \ , \tag{8}$$

where $\delta_0(\mathbf{x}) = \delta_0(x)\delta_0(y)$.

Proof. One possible definition of the 1D Dirac delta function is

$$\delta_0(x) = \begin{cases} 0 & \text{if } x \neq 0 \\ \infty & \text{if } x = 0 \end{cases} \qquad \text{and} \qquad \int_{\mathbb{R}} \delta_0(x)\, dx = 1 \ .$$

The 2D Dirac impulse is defined to be the product of the 1D Dirac impulses in x- and y-direction. Hence, the integral property changes to

$$\iint_{\mathbb{R}^2} \delta_0(\mathbf{x})\, d\mathbf{x} = 1 \ .$$

If $b = 0$ and $\mathbf{x} \neq 0$ we have $p(\mathbf{x}; b) = 0$. For $b > 0$, $p(0; b) = (2\pi b^2)^{-1}$ so that $\lim_{b \to 0} p(0; b) = \infty$. Furthermore,

$$\iint_{\mathbb{R}^2} p(\mathbf{x}; b)\, d\mathbf{x} = \int_0^{2\pi} \int_0^{\pi/2} p(\theta, \psi) = 1 \ .$$

In reality, however, the three assumptions made above are violated. At first, we omit the second assumption, i.e., the lens is finite. This corresponds to applying an *aperture*, i.e., a window function, to the Poisson blurred image in the lens plane. This window function is also projected onto any image plane. The intensity distribution which results from a single object point thus corresponds to a windowed Poisson-kernel-shaped intensity in the image plane. As long as the image of the object point is not too close to the window border, the effect of the aperture is hardly visible. However, the integral of the density is now less than one. Hence, the weight of the Dirac impulse at the point of focus is decreased. The decrement depends on the part of the Poisson kernel which is windowed out and increases with the distance of the object point to the optical axis. Therefore, points in the periphery of the visual field appear darker (*vignetting*).

Besides vignetting the finite lens (or an additional aperture) also have the *positive* effect, that the other two assumptions are not critical any more. The light emitted from a plane dull surface is known to be Lambertian, i.e., its intensity is proportional to the scalar product of the surface normal and the observation direction. If the width of the aperture is small compared to the distance to the object, the orientation dependent term can be neglected. Furthermore, the object need not be flat anymore, although the slope of the depth map must be less than the ration between the aperture width and the distance to the object for keeping the model valid. Although one could go on with further refinements of the model to more realistic settings, we conclude this motivating section at this point.

2.2   The Poisson Scale-Space

In this section we show that the Poisson kernel actually establishes a linear scale-space, since it fulfills the axiomatic from Section 1.2 (see also [13, 9]). Based on the motivation in the previous section, we now state the following theorem.

Theorem 1 (Poisson scale-space) *The Poisson kernel (7) establishes a linear, isotropic scale-space.*[5]

In order to prove this theorem, we need the Fourier transform of the Poisson kernel. The 2D Fourier transform is denoted by

$$\mathcal{F}_2\{f(\mathbf{x})\}(\boldsymbol{\xi}) = \iint_{\mathbb{R}^2} f(\mathbf{x})\exp(-i2\pi\,\boldsymbol{\xi}\cdot\mathbf{x})\,d\mathbf{x}$$

where $\boldsymbol{\xi} = (\xi,\eta)^T$ and $\mathbf{x} = (x,y)^T$.

Lemma 2 *The spectrum of the Poisson kernel (7) is given by*

$$\mathcal{F}_2\{p(\mathbf{x};b)\}(\boldsymbol{\xi}) = \exp(-2\pi|\boldsymbol{\xi}|b) \ . \tag{9}$$

Proof. See [38, 13] In the following we use the abbreviation $P(\boldsymbol{\xi};b) = \mathcal{F}_2\{p(\mathbf{x};b)\}(\boldsymbol{\xi})$. Now we give a proof that the Poisson kernel establishes a linear scale-space.
Proof (of Theorem 1).

- The axioms A1 and A2 are trivially fulfilled since $p(\mathbf{x};b)$ is an LSI operator, i.e., it is applied by means of convolutions.

- Axiom A3: We have

$$P(\boldsymbol{\xi};b_1)P(\boldsymbol{\xi};b_2) = \exp(-2\pi|\boldsymbol{\xi}|b_1)\exp(-2\pi|\boldsymbol{\xi}|b_2)$$
$$= \exp(-2\pi|\boldsymbol{\xi}|(b_1+b_2)) = P(\boldsymbol{\xi};b_1+b_2) \ ,$$

and hence $S(b_1,b_2) = b_1 + b_2$. In the spatial domain, this corresponds to $p(\mathbf{x};b_1) * p(\mathbf{x};b_2) = p(\mathbf{x};b_1+b_2)$.

- Axiom A4': Since

$$
\begin{aligned}
p(a\mathbf{R}\mathbf{x};b) &= \frac{b}{2\pi\left((a|\mathbf{R}\mathbf{x}|)^2 + b^2\right)^{3/2}} \\
&= \frac{1}{a^2}\frac{b/a}{2\pi\left(|\mathbf{x}|^2 + (b/a)^2\right)^{3/2}} = \frac{1}{a^2}p(\mathbf{x};b/a) \ ,
\end{aligned}
$$

---

[5]Note that the symbol Σ from (1) is replaced with b.

the observation transformation is scale and rotation invariant:

$$
\begin{aligned}
\Phi(f(a^{-1}\mathbf{R}^T\mathbf{x}'), \mathbf{x}, b) &= \iint_{\mathbb{R}^2} f(a^{-1}\mathbf{R}^T\mathbf{x}')p(\mathbf{x}-\mathbf{x}'; b)\, d\mathbf{x}' \\
&\text{substitute } \mathbf{x} = a\mathbf{R}\mathbf{t} \text{ and } \mathbf{x}' = a\mathbf{R}\mathbf{t}' \\
&= \iint_{\mathbb{R}^2} f(\mathbf{t}')p(a\mathbf{R}(\mathbf{t}-\mathbf{t}'); b)a^2\, d\mathbf{t}' \\
&= \iint_{\mathbb{R}^2} f(\mathbf{t}')p(\mathbf{t}-\mathbf{t}'; b/a)\, d\mathbf{t}' \\
&= \Phi(f(\mathbf{x}'), \mathbf{x}, b/a)\ .
\end{aligned}
$$

Hence $T(b, a) = b/a$.

- Axiom A5 is fulfilled since the Poisson kernel is positive for all $\mathbf{x}$: $p(\mathbf{x}; b) > 0$ for all $\mathbf{x} \in \mathbb{R}^2$ and all $b > 0$.

This proof also holds for other dimensions than two, especially in the 1D case [13]. Hence, we have found a counterexample of the uniqueness proof in [22]. At this point one might ask if the proof of Iijima contains an error. The answer is yes – Iijima assumes implicitly that the frequency response of the scale-space kernel is continuously differentiable in the origin (see appendix). However, according to [41] the original 2D axiomatic of Iijima in [23] is based on the axiom A4 instead of A4', i.e., closedness under the affine group is required. The Poisson kernel is not closed under the full affine group, and hence, it does no longer establish a linear scale-space. We will give a simple counterexample in the sequel. Consider the following transformations of the affine group, forming a subgroup:

$$
\mathbf{L} \in \mathrm{GL}(2) \qquad \text{with} \qquad \mathbf{L} = \mathbf{R}^T \begin{pmatrix} \lambda & 0 \\ 0 & \lambda^{-1} \end{pmatrix} \mathbf{R}\ , \tag{10}
$$

where $\mathbf{R} \in \mathrm{SO}(2)$. The considered subgroup deforms the image plane in an anisotropic way. Without loss of generality we can omit the rotation such that $\mathbf{L}$ is diagonal, i.e., the coordinate axes are rescaled by the subgroup. Furthermore assume that $\mathbf{L}_1 \neq \mathbf{L}_2$ are two elements of this subgroup. For *one* of these anisotropic deformations it is possible to define an anisotropic Poisson scale-space by a simple change of the coordinate system [13].[6] However, the combination of closedness under the affine group and the semigroup property implies that the convolution of *two affine transformed kernels* is again a kernel from the generating family. This is clearly violated in case of the Poisson kernel which is easiest shown in the frequency domain (see appendix). There is even a more fundamental relationship which we formulate as a theorem.

Theorem 2 (separability of observation transformation) *An observation transformation which fulfills the axioms A1-A5 is separable, i.e., fulfills axiom A7.*

---

[6]By an appropriate change of the coordinate system it is also possible to extend the Poisson scale-space to the full affine group.

Proof. From the axioms A1 and A2 one can conclude that the observation transformation is obtained by a convolution with a kernel $k(\mathbf{x}; \Sigma)$ [41]. The closedness under affine transformations (A4) and the semigroup property (A3) imply that

$$
\begin{aligned}
k((x, \varepsilon y)^T; \Sigma) &= k(\mathbf{x}; \Sigma_1) \\
k((\varepsilon x, y)^T; \Sigma) &= k(\mathbf{x}; \Sigma_2) \\
k((x, \varepsilon y)^T; \Sigma) * k((\varepsilon x, y)^T; \Sigma) &= k(\mathbf{x}; \Sigma_1) * k(\mathbf{x}; \Sigma_2) = k(\mathbf{x}; \Sigma_3)
\end{aligned}
$$

for any $\varepsilon > 0$. The case $\varepsilon \to 0$ corresponds to writing $k(\mathbf{x}; \Sigma_3)$ as a convolution of two 1D kernels, and hence, the kernel $k(\mathbf{x}; \Sigma)$ is separable.

As a counterpart of Theorem 2 one could state that any observation transformation which fulfills the axioms A1-A3,A4',A5 and A7, also fulfills the axiom A4. The proof is basically given in [33] where a one-parameter class of kernels with the frequency response $\exp(-2\pi|\boldsymbol{\xi}|^\alpha b)$, $\alpha \in (0, 2]$, is obtained. By the separability constraint we obtain $\alpha = 2$, i.e., the Gaussian kernel becomes the only solution. The Gaussian kernel is closed under the affine group.

As a quintessence of the preceding discussion we conclude that replacing the axiom A4' with A4 is equivalent to adding axiom A7. Hence, the difference between the axiomatic yielding the Gaussian kernel as the unique solution and the axiomatic yielding a family of kernels as solutions (a.o. the Poisson kernel) boils down to separability. In other words: the only difference between the Poisson kernel and the Gaussian kernel with respect to the axiomatics is the separability.

2.3   The Analytic and Monogenic Scale-Space Representations

The Poisson kernel (7) is closely related to the Laplace equation (or potential equation)

$$
\Delta_3 u(x, y, b) = u_{xx}(x, y, b) + u_{yy}(x, y, b) + u_{bb}(x, y, b) = 0 \ . \tag{11}
$$

Informally, the Poisson kernel is the *fundamental solution* of the 'square root' of the Laplace equation. To make this point more evident, consider the fundamental solution[7] of the Laplace equation:

$$
\varphi(x, y, b) = -\frac{1}{4\pi\sqrt{x^2 + y^2 + b^2}} \ , \tag{12}
$$

i.e., $\Delta_3\varphi(x, y, b) = \delta_0(x, y, b) = \delta_0(x)\delta_0(y)\delta_0(b)$ (this can easily be checked using the divergence (or Gauss) theorem). A scalar function $u(x, y, b)$ which fulfills the Laplace equation is called a harmonic function (harmonic potential). The gradient field of a harmonic function $\mathbf{f}(x, y, b) = \nabla_3 u(x, y, b)$ is known to be irrotational and divergence free, i.e.,

$$
\begin{aligned}
\operatorname{curl} \mathbf{f}(x, y, b) &= \nabla_3 \times \mathbf{f}(x, y, b) &= 0 \\
\operatorname{div} \mathbf{f}(x, y, b) &= \nabla_3 \cdot \mathbf{f}(x, y, b) &= 0
\end{aligned} \ , \tag{13}
$$

---

[7]Actually the constant $-(4\pi)^{-1}$ is an arbitrary choice, any other constant is a valid choice [6], page 209. However, due to normalization of the Dirac impulse, we prefer the given constant.

where $\nabla_3 = (\partial_x, \partial_y, \partial_b)^T$ is the 3D gradient operator. Since $\nabla_3 \cdot \nabla_3 = \Delta_3$, the gradient operator can be considered as the 'square root' of the Laplace operator. Furthermore, $\varphi(x, y, b)$ is the fundamental solution of the Laplace equation, and hence, $\nabla\varphi(x, y, b)$ is obviously the fundamental solution of the system of equations in (13). However, considering this fundamental solution yields

$$
\begin{array}{rcl}
\partial_x\varphi(x, y, b) & = & \dfrac{x}{4\pi(x^2 + y^2 + b^2)^{3/2}} \\[2mm]
\partial_y\varphi(x, y, b) & = & \dfrac{y}{4\pi(x^2 + y^2 + b^2)^{3/2}} \\[2mm]
\partial_b\varphi(x, y, b) & = & \dfrac{b}{4\pi(x^2 + y^2 + b^2)^{3/2}}
\end{array}
\quad , \tag{14}
$$

i.e., the Poisson kernel is one component of the fundamental solution of (13) (up to a factor of two).

Returning to the original setting of scale-space representation, the considered problem is a boundary value problem on the half space $b > 0$. The appropriate method to get the solution of such a problem is the Schwarz reflection principle, which leads to a factor of two in the fundamental solution (see e.g. [6], page 279). Hence, the Poisson kernel is one component of the fundamental solution of (13) in the half space $b > 0$.

In a next step, we separate the image plane from the scale axis. In particular, we rewrite $\mathbf{f}(x, y, b) = (\mathbf{v}^T(\mathbf{x}; b)\ u(\mathbf{x}; b))^T$, i.e., $\mathbf{v}(\mathbf{x}; b)$ is a vector field $\mathbb{R}^2 \oplus \mathbb{R}^+ \to \mathbb{R}^2$, and we obtain a new set of equation from (13):

$$
\begin{array}{rcl}
\operatorname{curl} \mathbf{v}(\mathbf{x}; b) & = & 0 \tag{15} \\[2mm]
\nabla_2 \cdot \mathbf{v}(\mathbf{x}; b) + \partial_b u(\mathbf{x}; b) & = & 0 \tag{16} \\[2mm]
\partial_b \mathbf{v}(\mathbf{x}; b) - \nabla_2 u(\mathbf{x}; b) & = & 0 \tag{17}
\end{array}
$$

for all $b > 0$ and $\nabla_2 = (\partial_x, \partial_y)^T$. Obviously, the zero divergence in (13) yields the 2D continuity equation (16) which is also referred to in case of the Gaussian scale-space.

However, in contrast to the Gaussian scale-space, we do not combine the continuity equation (16) with Fick's law [40] or the maximum loss of figure impression (axiom A6) [41] yielding the figure flow. In the current framework, the figure flow is replaced with $\mathbf{v}(\mathbf{x}; b)$ which is already implicitly determined by means of (13). The relationship between $u(\mathbf{x}; b)$ and $\mathbf{v}(\mathbf{x}; b)$ is given by the Riesz transform [38, 10], a 2D generalization of the Hilbert transform [15] with the vector-valued frequency response and impulse response, respectively,

$$
\mathbf{H}(\boldsymbol{\xi}) = i\frac{\boldsymbol{\xi}}{|\boldsymbol{\xi}|} \qquad \mathbf{h}(\mathbf{x}) = -\frac{\mathbf{x}}{2\pi|\mathbf{x}|^3} \quad . \tag{18}
$$

Hence, the figure flow/image flux is replaced with the Riesz transform of the image.

The combination of a signal with its Riesz transform forms a 2D generalization of the analytic signal, the monogenic signal [15]:

$$
\mathbf{f}_{\mathrm{M}}(\mathbf{x}) = ((\mathbf{h}^T * f)(\mathbf{x})\ f(\mathbf{x}))^T \quad . \tag{19}
$$

Thus, using the Poisson kernel for generating a linear scale-space arises from combining the monogenic signal with the continuity equation (16). This underpins the special role of the Poisson scale-space: It is derived from an optical setting (defocusing) which implies the continuity equation and stands in direct relation to the monogenic signal. The latter yields a quadrature filter approach if it is combined with radial bandpass filters, which in turn can be considered as a concept from scale-space. The same is true in the 1D case, where the 'image' (signal) flux obtained from the 1D Poisson scale-space is given by the Hilbert transform of the signal.

For convenience, we introduce two new terms:

Definition 2 (analytic scale-space) *The Poisson scale-space representation of a 1D analytic signal is called the 1D analytic scale-space representation.*

Note that the 1D analytic scale-space representation is formed by the 1D Poisson scale-space representation of a signal and the corresponding signal flux. It is an analytic function in the upper half-plane $b > 0$.

Definition 3 (monogenic scale-space) *The Poisson scale-space representation of a 2D monogenic signal is called the 2D monogenic scale-space representation.*

Note that the 2D monogenic scale-space representation is formed by the 2D Poisson scale-space representation of a signal and the corresponding image flux. It is a *monogenic* function in the upper half-space $b > 0$. Monogenic functions are solutions of the generalized Cauchy-Riemann equations, known from Clifford analysis [4]. Since we only consider (para-)vector valued functions, the here considered monogenic functions are equivalent to 3D vector fields with zero divergence and zero curl.

In the current context it does not matter from which side of the theory one approaches the problem. Also starting from the derivation of the Riesz transform (see [15, 13]) yields the Poisson scale-space. Furthermore, due to the theory of monogenic functions, the same 3D Euclidean space is used for embedding the 2D scale-space and for representing the quadrature filter output. In particular, this imposes an identification of the image plane coordinates with the Riesz components, or the image flux components, and this imposes an identification of the scale axis with the applicate axis, i.e., the signal value axis.

2.4   Relaxed Causality

The causality of scale-space representation (axiom A8) was introduced in [25] as a fundamental concept. Therein causality is defined by the statement: 'any feature at a coarse level of resolution is required to possess a (not necessarily unique) "cause" at a finer level of resolution although the reverse need not be true.' The subsequent formal treatment however, is slightly stricter, and it requires that the convex side of an isophote in an extremum points towards coarser scales (axiom A9). This requirement is basically the same as the non-enhancement of local extrema [1, 30].

The non-enhancement property is only fulfilled in the case of the Gaussian scale-space [1], and therefore the Poisson scale-space does not fulfill the causality requirement in its

stricter formulation, see also Figure 3. However, motivated by the relationship between causality and the maximum principle [20][8], we use the original informal definition of causality to prove that the Poisson scale-space is causal in a relaxed sense.
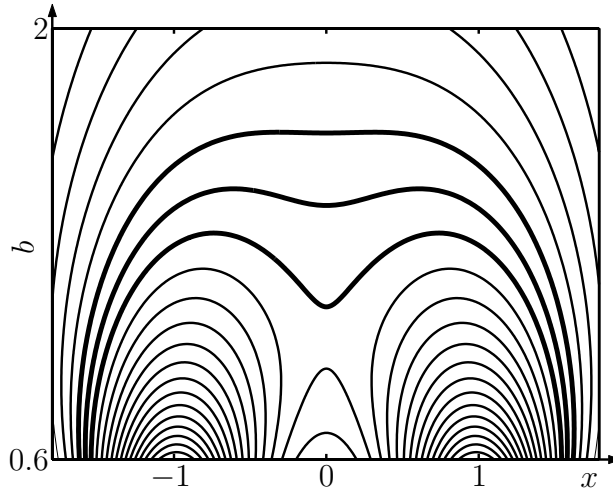

Figure 3: Example due to [1], showing that the 1D Poisson scale-space does not fulfill the non-enhancement axiom A9.

Definition 4 (relaxed causality) *A scale-space representation $u(\mathbf{x}; b)$ is called causal in a relaxed sense, if any level crossing surface, i.e., any connected component of $u(\mathbf{x}; b) = \lambda$, $\lambda \in \mathbb{R}$, is connected to a point $u(\mathbf{x}; 0) = \lambda$.*

In order to illustrate the two different definitions of causality, we switch to 1D scale-space. In the Figure 4 four different cases of isophotes are illustrated. According to the two
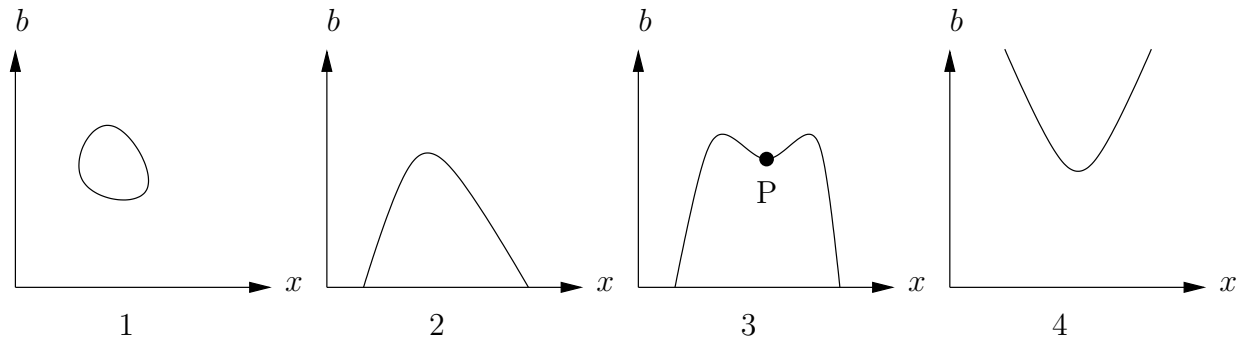
Figure 4: Causality in 1D scale-space. The two definitions only differ with respect to the third case.

different definitions of causality, we obtain the following categorization:

1. The isopleth is closed for $b > 0$. We do not have causality in the strict sense, since the convex side also points towards finer scales. We also do not have causality in the relaxed sense, since the surface is not connected to a point on the line $b = 0$.

2. The isopleth is connected to the line $b = 0$ and it is convex wrt. to increasing scale. Hence, we have causality according to both definitions.

3. The isopleth is connected to the line $b = 0$ but it is not convex wrt. increasing scale for all x, it is concave in the point P. In this case we only have causality in the relaxed sense.

4. The isopleth is not closed and not connected to the line $b = 0$. We do not have strict causality since the surface is concave. We do not have relaxed causality either since the surface is not connected to the line $b = 0$.

Actually, there are other possible cases like open surfaces which intersect the line $b = 0$ in only one point, but those are not relevant for the current discussion. The main difference between the two definition of causality boils down to the third case. Whereas strict causality requires the isopleth to be connected to the plane $b = 0$ in the space 'between' the current scale and scale zero, the relaxed causality only requires connectivity in the whole half-space $b > 0$.

Relaxing the causality requirement according to Definition 4 enables us to categorize the Poisson scale-space to be causal although it does not fulfill the non-enhancement property.

Theorem 3 (causality of Poisson scale-space) *The Poisson scale-space representation of a DC-free 2D signal in $\mathbb{L}_1$ fulfills the causality requirement according to Definition 4.*

Proof. The proof consists of two parts. First, we show that there exists no closed level crossing surface for $b > 0$. Second, we show that any open level crossing surface intersects the plane $b = 0$. The Poisson scale-space representation is denoted by $u(\mathbf{x}; b)$.

Assume that there exists a closed level crossing surface c_λ given by a connected component of $u(\mathbf{x}; b) = \lambda$, $\lambda \in \mathbb{R}$ and $b > 0$. Since the Poisson kernel is differentiable for $b > 0$, $u(\mathbf{x}; b)$ is also differentiable for $b > 0$. Hence, there exists an $\varepsilon > 0$ such that a connected component $c_{\lambda+\varepsilon}$ of $u(\mathbf{x}; b) = \lambda + \varepsilon$ or $c_{\lambda-\varepsilon}$ of $u(\mathbf{x}; b) = \lambda - \varepsilon$ are level crossings which lie entirely outside the level crossing c_λ (see Figure 5). Without loss of generality we assume that $c_{\lambda+\varepsilon}$ lies entirely outside c_λ. Due to the maximum principle of harmonic functions [27], we know that $u(\mathbf{x}; b) = \lambda + \varepsilon$ inside of $c_{\lambda+\varepsilon}$ which yields a contradiction.

Knowing that all level crossings must be open, we just have to show that each of them is connected to the plane $b = 0$. Since both the original signal and the Poisson kernel are in $\mathbb{L}_1$, $u(\mathbf{x}; b)$ is in $\mathbb{L}_1$ for each $b \geq 0$, too. Hence, $\lim_{|\mathbf{x}| \to \infty} u(\mathbf{x}; b) = 0$ for each $b \geq 0$. Furthermore, $\lim_{b \to \infty} p(\mathbf{x}; b) \equiv 0$, and hence $\lim_{b \to \infty} u(\mathbf{x}; b) \equiv 0$. Thus all level-crossings with $\lambda \neq 0$ are connected to the plane $b = 0$. There might exist zero-crossings which are connected to the planes given by $b \to \infty$ and $|\mathbf{x}| \to \infty$, but these planes are connected to each other and especially to the line given by $|\mathbf{x}| \to \infty$ and $b = 0$, which is part of the plane $b = 0$.

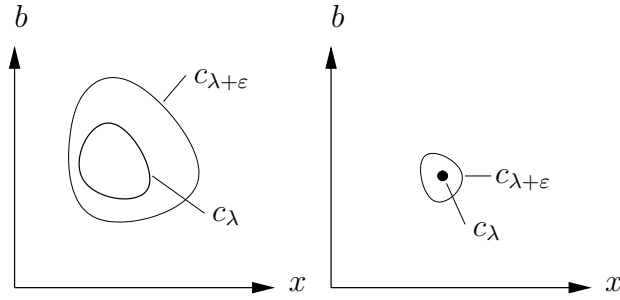Figure 5: Level crossings at the levels c_λ and $c_{\lambda+\varepsilon}$ illustrating the argumentation in the proof of Theorem 3.

2.5 Further Properties

In this section, we compare the Poisson scale-space to the Gaussian scale-space with respect to several properties.

It is well known that the non-creation of local extrema in the case of the 1D Gaussian scale-space does not generalize to higher dimensions [29]. Instead of considering the creation of local extrema, the authors in [1] consider (zero-crossing) contours, showing that these contours can merge and split with increasing fine scale. We adapted their example of the 'dumbbell' (Figure 6, left) to illustrate the corresponding property of the Poisson scale-space. Same as for the Gaussian case, the contours can split and merge, see Figure 6, right.
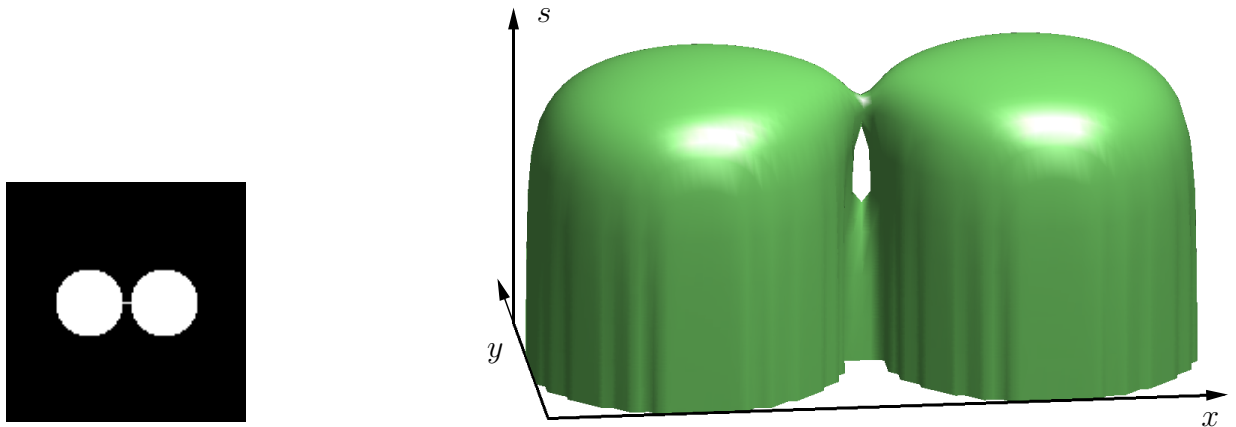
Figure 6: Test pattern from [1] (left) and a resulting level-crossing surface in scale-space (right).

Like for the Gaussian scale-space, the Poisson scale-space representation can be used to interpret images in term of singularities, extrema, saddle-points, etc. (see [25]). However, for the Poisson scale-space a new systematic evolves. The 1D Poisson scale-space is closely

related to the Laplace transform [36] (and therefore to the Z-transform), which give rise to signal representation and interpretation in terms of zeros and poles. In [13] it is shown that the spectrum of an analytic signal in the Poisson scale-space is given by the one-sided Laplace transform of the original spectrum. Hence, the zeros and poles in the spatial domain completely represent the original spectrum. Generalizing this idea to 2D, it is reasonable that the zero-crossings, singularities, and saddle-points in scale-space completely represent the original spectrum. However, the corresponding systematic for the 2D Poisson scale-space is not completely derived yet, although we make some considerations about the zeros in monogenic scale-space in Section 3.3.

Besides the behavior of the signal in scale-space, it is also reasonable to compare the two involved convolution kernels. The Gaussian kernel is known to be the only real-valued operator with the optimal uncertainty of $(2\pi)^{-1}$, [2, 32]. The uncertainty of the Poisson kernel is just slightly worse (by a factor of $\sqrt{1.5}$, see appendix). This slight increase of uncertainty is caused by the larger extent of the Poisson kernel in both domains, see Figure 7. For the sake of simplicity, the figure shows the comparison for the 1D case, but it is basically the same for 2D, see [13]. To compare both kernels, the maximum of the Poisson kernel is chosen to be the same as the one of the Gaussian kernel ($b = \sqrt{2}\sigma/\sqrt{\pi}$ [13]).
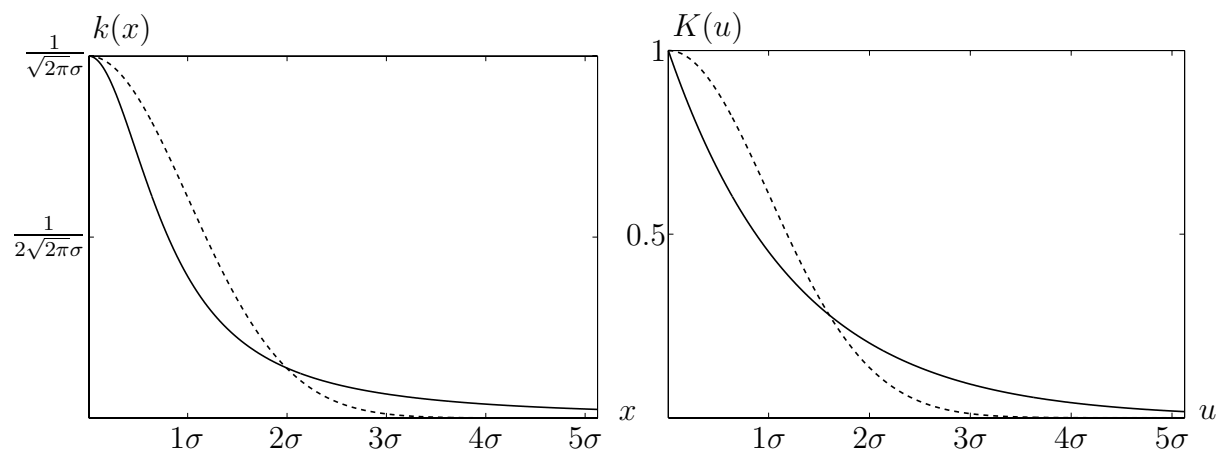

Figure 7: The 1D Gaussian kernel (dashed line) and the 1D Poisson kernel (solid line) in spatial domain (left) and frequency domain (right). All axes are labeled relative to the standard deviation σ of the Gaussian.

Besides the axioms and properties we have verified in this section, there are a tile of further axioms which are considered in the context of the Poisson kernel in [10, 9, 33]. We now focus on the relationship between the Poisson scale-space and phase-based image processing.

3   The Local Phase in Scale-Space

In the preceding sections of this paper, we have shown that the Poisson scale-space is a quite good alternative to the Gaussian scale-space. However, there are more alternatives [10] and it is legitimate to ask why to change existing methods using the Gaussian kernel. For many applications it is appropriate to keep with the Gaussian kernel, however, there are cases where it might be advantageous or even necessary to switch to the Poisson scale-space. One of the latter cases arises if the ideas of local phase and scale-space are combined to recognize local structures and to measure local features. The direct relationship between the Poisson scale-space and the monogenic signal (see Section 2.3) yields new possibilities of phase-based image processing in scale-space. To show the advantages of a common framework for a quadrature concept and a scale-space approach, we start with a simple application: edge detection by differential phase congruency. In the subsequent sections, we derive a 2D generalization of the attenuation-phase relationship based upon intrinsically 1D monogenic signals. This relationship is exploited in the last section to compare phase-based and amplitude-based approaches.

3.1   Differential Phase Congruency

Edge detection by means of quadrature filters can be performed in two ways: either by detecting local maxima of the local amplitude or by detecting points of stationary phase in scale-space. The latter approach is commonly called *phase congruency* and is based on comparisons of the local phase at certain distinct scales [26, 35]. The obvious drawbacks of using several scales are:

- Edges are scale-relative, i.e., they have a certain optimal scale for detection and have a limited extent in scale-space.

- If an edge vanishes at a certain scale *between* two considered scales, it might not be reported. The choices of the distance between the considered scales and of the number of scales are quite critical parameters.

- Due to sampling of the orientation and of the scale, a large number of basis filters has to be applied, yielding a high computational complexity.

In [14] we presented a phase congruency based edge detector which makes use of the monogenic signal. Although that method is already much faster than the classical methods cited above, the drawback concerning the choice of scales is still valid. In [13] an advanced method has be developed based on the idea of differential phase congruency.

   The differential phase congruency replaces the finite difference of phases on different scales by a scale-derivative of the phase, i.e., differential phase congruency is given if $\partial_b \mathbf{r} = 0$, where $\mathbf{r}$ denotes the local phase-vector (see below). Due to the common framework of the quadrature approach and the Poisson scale-space, i.e., the monogenic scale-space, it is possible to derive a filter set such that it is not necessary to compute the b-derivative

explicitly. Instead, the phase congruency is computed at a certain scale, speeding up the computation by factor three or four.

The b-derivative can be computed as follows: The phase vector $\mathbf{r}$ of the monogenic scale-space is defined by

$$\mathbf{r}(\mathbf{x};b) = \frac{\mathbf{v}(\mathbf{x};b)}{|\mathbf{v}(\mathbf{x};b)|} \arctan\left(\frac{|\mathbf{v}(\mathbf{x};b)|}{u(\mathbf{x};b)}\right) \quad , \tag{20}$$

where $\arctan(\cdot) \in [0,\pi)$. Now assume that we have an edge or line, imposing that the phase does not change through scale on a certain interval. In terms of the b-derivative of $\mathbf{r}$, this means that this derivative is zero. Furthermore, the term $\mathbf{v}/|\mathbf{v}|$ describes the local orientation [15] which is also independent of b at a line or edge. Hence, we can rewrite $\mathbf{v}$ as $v\mathbf{n} = v(\cos\theta, \sin\theta)^T$ for appropriate θ and $v \geq 0$. The b-derivative of $\mathbf{r}$ then reads

$$\begin{aligned}
\partial_b \mathbf{r}(\mathbf{x};b) &= \mathbf{n}\partial_b \arctan\left(\frac{v(\mathbf{x};b)}{u(\mathbf{x};b)}\right) \\
&= \frac{\mathbf{n}(u(\mathbf{x};b)\partial_b v(\mathbf{x};b) - v(\mathbf{x};b)\partial_b u(\mathbf{x};b))}{u(\mathbf{x};b)^2 + v(\mathbf{x};b)^2} \\
&= \frac{u(\mathbf{x};b)\partial_b \mathbf{v}(\mathbf{x};b) - \mathbf{v}(\mathbf{x};b)\partial_b u(\mathbf{x};b)}{u(\mathbf{x};b)^2 + |\mathbf{v}(\mathbf{x};b)|^2} \quad .
\end{aligned} \tag{21}$$

Note that the b-derivatives of the monogenic scale-space can be computed without using discrete approximations. This is done by replacing the Poisson kernel with its b-derivative. The result is a set of three further linear filters (the derivative of the Poisson kernel and the derivatives of the two components of its Riesz transform) which are applied to the signal at the original scale. The outputs are combined with the output of the original kernels according to (21). In contrast to the Gaussian framework, the Poisson scale-space allows to compute all involved kernels in both domains, the spatial domain and the frequency domain. This can be of great importance in certain cases of optimized filter design. Furthermore, the b-derivatives can also be replaced with $\mathbf{x}$-derivatives (see (16) , (17), and Section 3.4), which is also unique to the Poisson framework.

Returning to the points of phase congruency, we have to find the zeros of the two components of (21). By a linear regression, these zeros can easily be detected with subpixel accuracy. After removing those zeros where the slope of (21) is smaller than a threshold, the results in Figure 8 are obtained.

3.2 The Local Attenuation – Local Phase Relationship in 1D

The 1D attenuation-phase relationship (see e.g. [31], page 206), states that for a minimum-phase system, the attenuation (logarithm of the amplitude response) and the phase response are related by the Hilbert transform.

In order to explore the background of this relationship, we consider an analytic function $w(z)$ which is non-zero everywhere. Hence, $\log(w(z))$ is also analytic and non-singular, which can easily be checked using the Cauchy-Riemann equations. Considering the Laplace
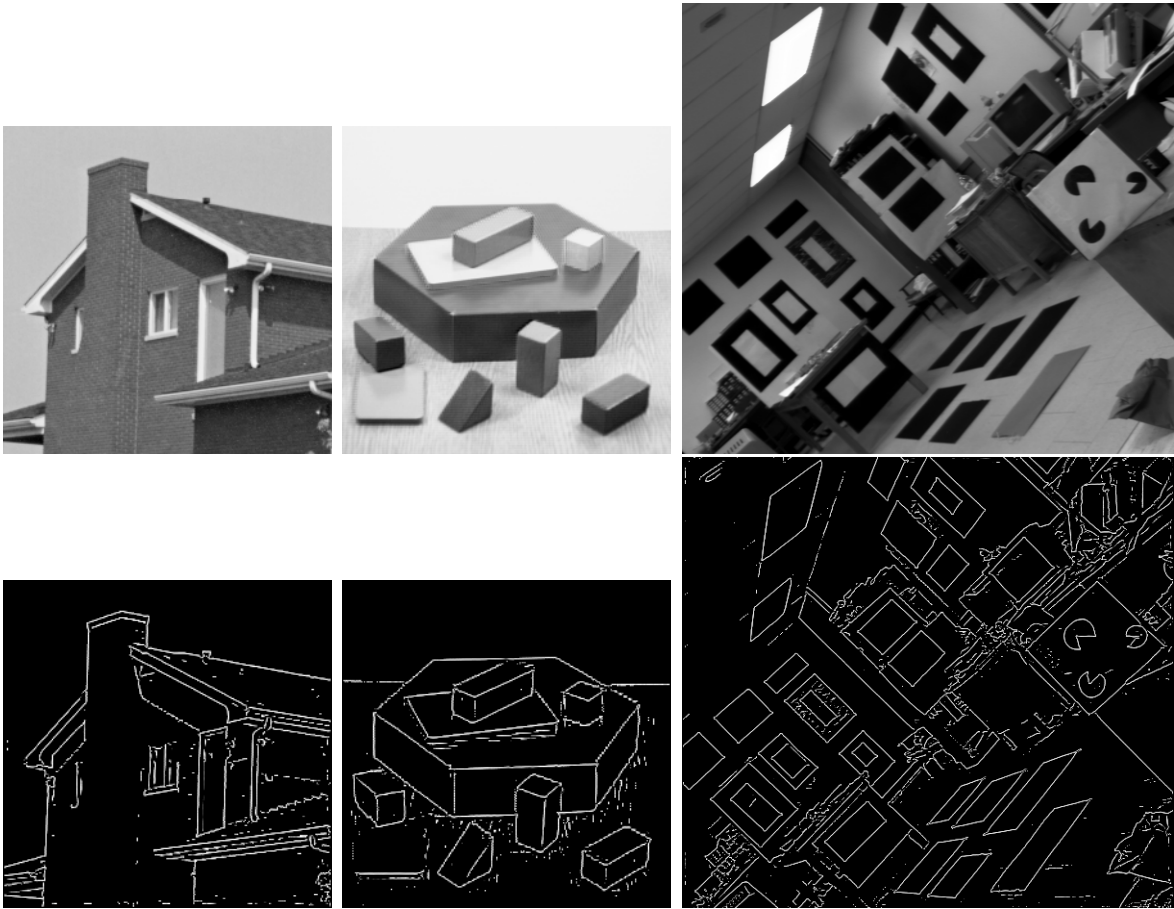
Figure 8: Results from differential phase congruency. Upper row: original images. Bottom row: detected edges and lines (same parameters for all images). For the purpose of comparison, see [13].

transform of a causal system, its transfer function is analytic in the positive half-plane. Hence, attenuation and phase response form an analytic function in this half-plane if the filer is minimum-phase, i.e., its transfer function has no zeros in the positive half-plane.

For the 1D analytic scale-space representation, the roles of Fourier domain and spatial domain are just exchanged [13]. Hence, the 1D analytic scale-space is an analytic function and if there are no zeros for positive scale parameters, the logarithm of the local amplitude, which we call *local attenuation*, and the local phase form a Hilbert pair for each scale. Unfortunately, zeros can occur for positive scale parameters, as it can be seen in Figure 9.

In order to investigate the conditions for zeros occurring in the analytic scale-space representation, we consider some simple 1D examples. For some elementary signals, like e.g. rectangle, triangle, no common zeros of the real part and the imaginary part exist, and therefore, the local attenuation and the local phase form a Hilbert pair. However, as
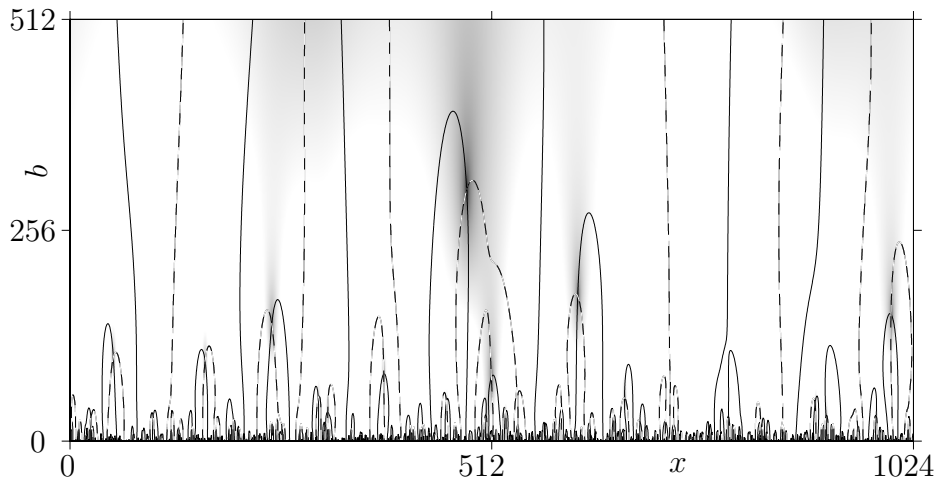
Figure 9: 1D Poisson scale-space: zeros of the local amplitude of a random signal. The zero-crossings of the real part are indicated by solid lines, the zero-crossings of the imaginary part are indicated by dashed lines. The grey-scale image in the background shows the (rescaled) local amplitude. Note that a zero of the local amplitude implies both parts, the real one and the imaginary one, to be zero.

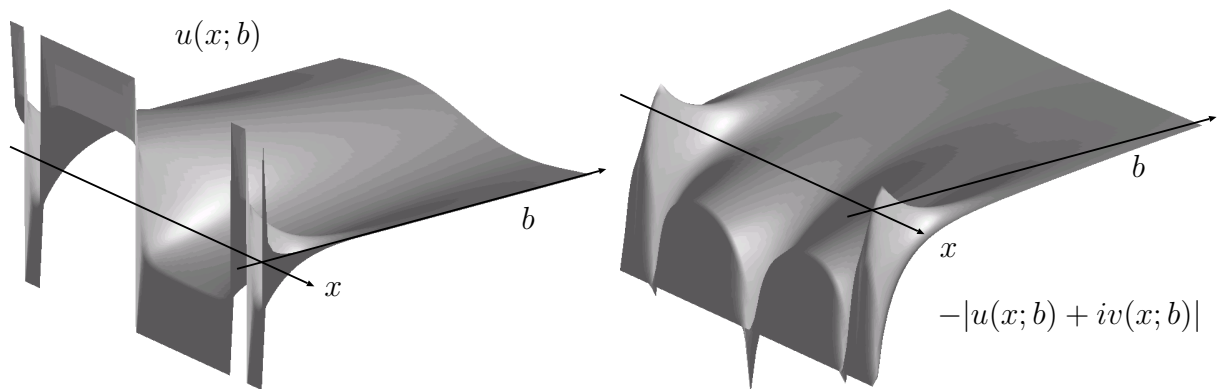soon as we combine two rectangles with different widths, zeros occur (see Figure 10).

Figure 10: Left: a combination of two rectangles in Poisson scale-space. Right: the corresponding local amplitude shows two zeros.

According to the well known approach of separating the frequency response of a general filter into an allpass part and a minimum-phase part, we factorize the analytic scale-space representation into one part which contains no zeros for $b > 0$ and one part with constant amplitude for $b = 0$ (see Figure 11).

For the part without zeros, the relationship between the local attenuation and the local phase is given by the Hilbert transform. The remaining part is fully characterized by the
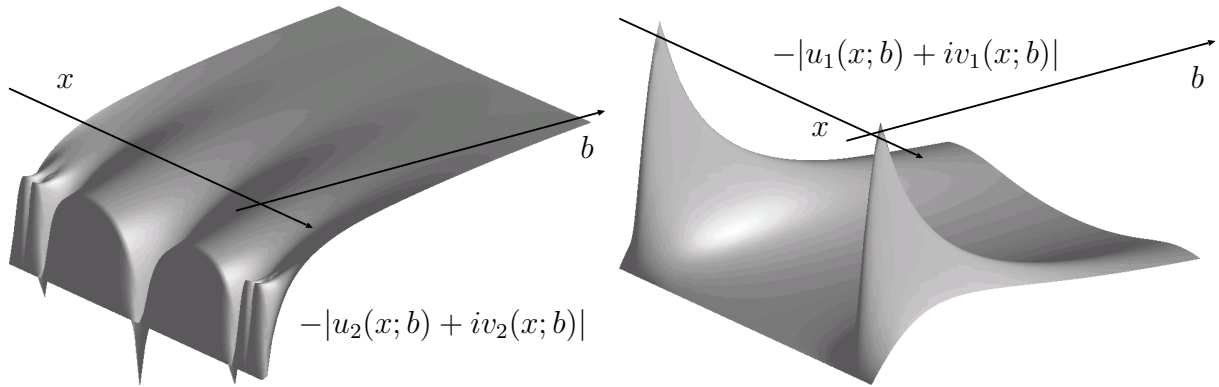
Figure 11: Left: local amplitude of factor without zeros. Right: remaining factor.

positions of the two zeros, which themselves indicate the positions of the steps between the two narrow rectangles (see also Figure 10, left). In general however, the zeros in the half-plane $b > 0$ cannot be directly related to signal structures in such a straightforward way. Furthermore, for the purpose of relating local attenuation and local phase *on a single scale or on a finite scale interval*, it is not reasonable to factor out all existing zeros, which requires to compute the full scale-space.

The influence of zeros is significantly reduced if the original signal is filtered with a bandpass beforehand. For estimating an appropriate local phase, it is anyhow necessary to have a well defined local frequency, or more realistic, a small bandwidth [19], page 171. To illustrate the effect of bandpass filtering, we apply a bandpass filter to the original test signal and compute the analytic scale-space representation (see Figure 12).
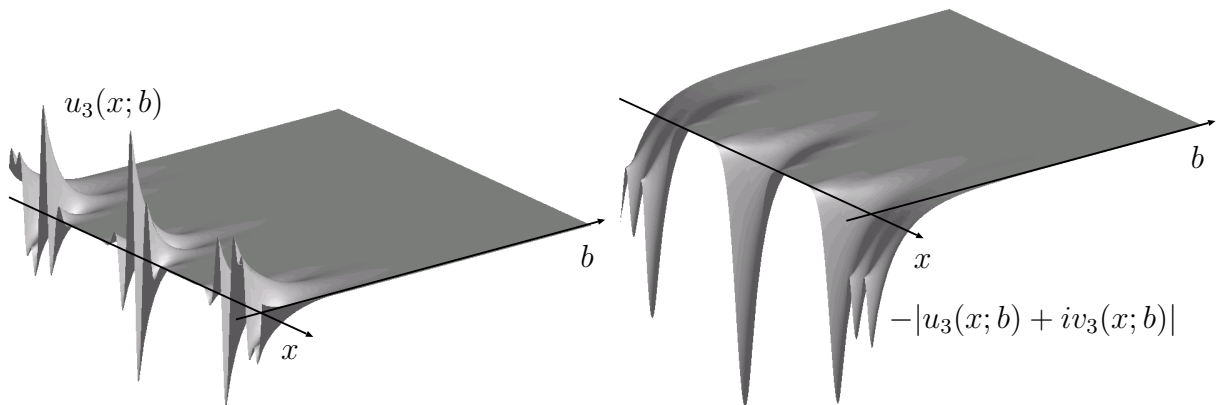

Figure 12: Left: real part of band-limited version of original signal. Right: local amplitude of this band-limited signal in scale-space.

Obviously, there occur no zeros for $b > 0$ in this example.[9] Thus, the attenuation-

---

[9] Although the local amplitude approaches zero for $b \to \infty$, there occur no critical points. These points

phase relationship applies to this bandpass filtered signal. Unfortunately, this is not true in general. If the signal contains two different frequency components which both lie in the passband of the bandpass filter, the smoothing process is reduced to a change of the relative weight between them. Hence, through scale-space, the number of oscillations (and therefore the number of zeros) can change, and therefore some zero-crossings must intersect (see Figure 13). This remains true for arbitrary small frequency differences – in order to
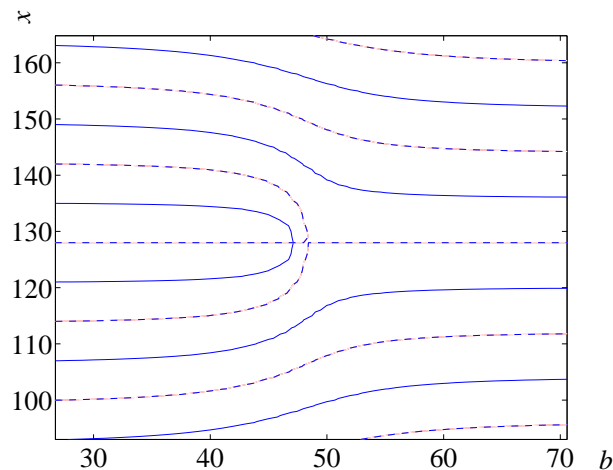

Figure 13: Intersecting zeros of real part (solid line) and imaginary part (dashed line) for a simple linear combination of two oscillations.

find intersecting zero-crossings one has to consider accordingly larger x-intervals.

Apart from this theoretic discussion about the validity of the relationship between local attenuation and local phase, we want to stress that the method works reliable in practice, at least in the 2D case, as we will show.

3.3 The Local Attenuation – Local Phase Relationship in 2D

For the 2D monogenic signal, the local phase is replaced with a phase vector, see (20). The local amplitude is given by the square-root of the sum of $u(\mathbf{x}; b)^2$ and $|\mathbf{v}(\mathbf{x}; b)|^2$ [15] and hence, the 2D local attenuation is given by

$$a(\mathbf{x}; b) = \frac{1}{2} \log(u(\mathbf{x}; b)^2 + |\mathbf{v}(\mathbf{x}; b)|^2) \ . \tag{22}$$

The topic of this section is the relationship between the 2D attenuation and the 2D phase vector and the corresponding requirements to the signal. We summarize this relationship in a theorem.

---

require to lie on a zero *crossing* of both parts, the real part and the imaginary part. In the present example, no such zero crossings intersect. Strictly spoken, it is also critical to have asymptotic zeros [21], but in case of finite scales, the asymptotic case is not relevant.

Theorem 4 (2D local attenuation and 2D local phase) *Let f be a 1D function in $\mathbb{L}_1$ such that its 1D analytic scale-space representation has no zeros in the plane $b > 0$ and let $\mathbf{n} \in \mathbb{R}^2$ with $|\mathbf{n}| = 1$. Furthermore, let $u(\mathbf{x}; b)$ be the 2D scale-space representation of $f(\mathbf{n} \cdot \mathbf{x})$ and let $\mathbf{v}(\mathbf{x}; b)$ be the corresponding image flux. Then the local attenuation (22) and the local phase vector (20) are related by the Riesz transform.*

Proof. Since $f(\mathbf{n} \cdot \mathbf{x})$ is constant in the perpendicular direction $\mathbf{n}^\perp$ of $\mathbf{n}$, we focus on the projections (integrals) onto the plane spanned by $\mathbf{n}$ and b. From the Fourier slice theorem [3] it follows that the 1D projections of the 2D Poisson kernel and the 2D Riesz kernel are identical to the 1D Poisson kernel and the Hilbert kernel (multiplied with $\mathbf{n}$), respectively:

$$\int_{-\infty}^{\infty} \frac{b}{2\pi(|s\mathbf{n} + t\mathbf{n}^\perp|^2 + b^2)^{3/2}} \, dt \;=\; \frac{b}{\pi(s^2 + b^2)}$$

$$\int_{-\infty}^{\infty} -\frac{s\mathbf{n} + t\mathbf{n}^\perp}{2\pi|s\mathbf{n} + t\mathbf{n}^\perp|^3} \, dt \;=\; -\frac{\mathbf{n}}{\pi s} \;,$$

where we made use of $\mathbf{x} = s\mathbf{n} + t\mathbf{n}^\perp$. Thus, all 2D convolutions of $f(\mathbf{n} \cdot \mathbf{x})$ with either the Poisson kernel or the Riesz kernel can be replaced with 1D convolutions with the 1D Poisson kernel and the Hilbert kernel (multiplied with $\mathbf{n}$). Hence, we know that the 2D monogenic scale-space of $f(\mathbf{n} \cdot \mathbf{x})$ is given by the 1D analytic scale-space of f if we multiply the 1D signal flux by $\mathbf{n}$. Moreover, the attenuations in both cases are the same. The phase vector according to (20) is given by $\mathbf{n}$ times the 1D phase [15], i.e., the phase vector and the 1D phase only differ by $\mathbf{n}$. Since the phase is the Hilbert transform of the 1D attenuation, the phase vector is obtained from the 2D attenuation by the projected Riesz transform. Returning to the original domain completes the proof.

Before we focus on the problem of zeros in the positive half space, we want to make some remarks.

1. The 2D signals which are obtained by projecting some 1D function f are called *intrinsically 1D* (i1D) [28] or *simple* [19] signals.

2. Although real images are not i1D signals in general, they are commonly composed of various regions which are locally i1D, i2D, or constant. However, the fast decrease of the Poisson kernel and the Riesz kernel with increasing radius ensures that the error caused by a finite integration (projection) is small.

3. For locally i2D regions the theorem does not hold in general.

4. The finite extent of locally i1D regions weakens the requirement of having no zeros in the positive halfplane (see below).

5. In practice one can use the 2D attenuation – phase vector relationship without testing for zeros.

Concerning the zeros in the 1D analytic scale-space of f, one would expect to meet lines which are zero in the 2D monogenic scale-space of i1D signals. However, due to the finite extent of i1D regions in real images, these lines mostly shrink to points or small line segments, see Figure 14 and 15. The areas indicated as zero in the right figures are
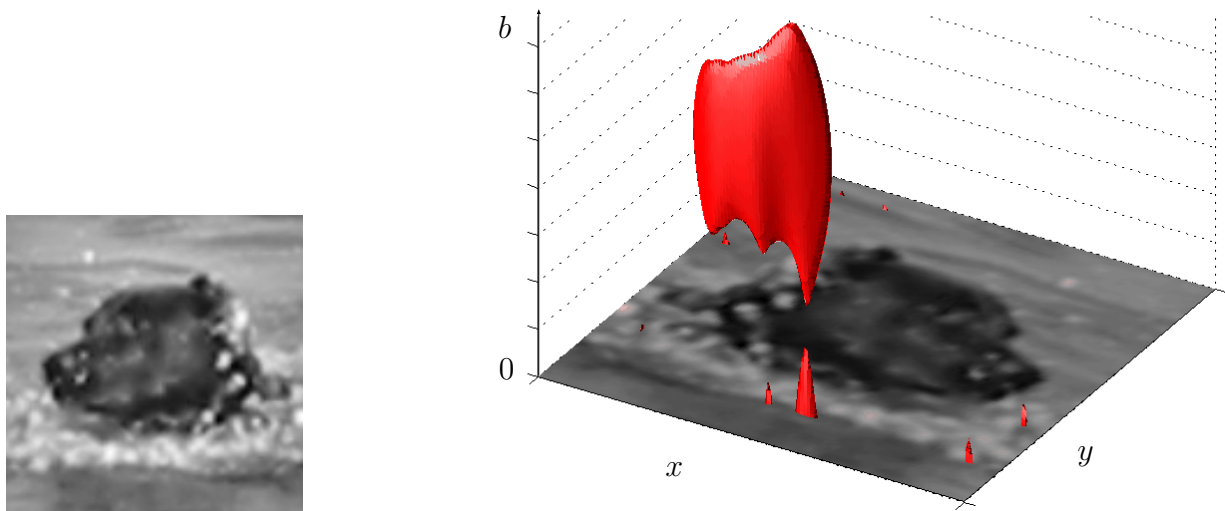

Figure 14: Zeros of dog image in monogenic scale-space. Left: original image, right: zeros (isophotes of finite, small amplitude).
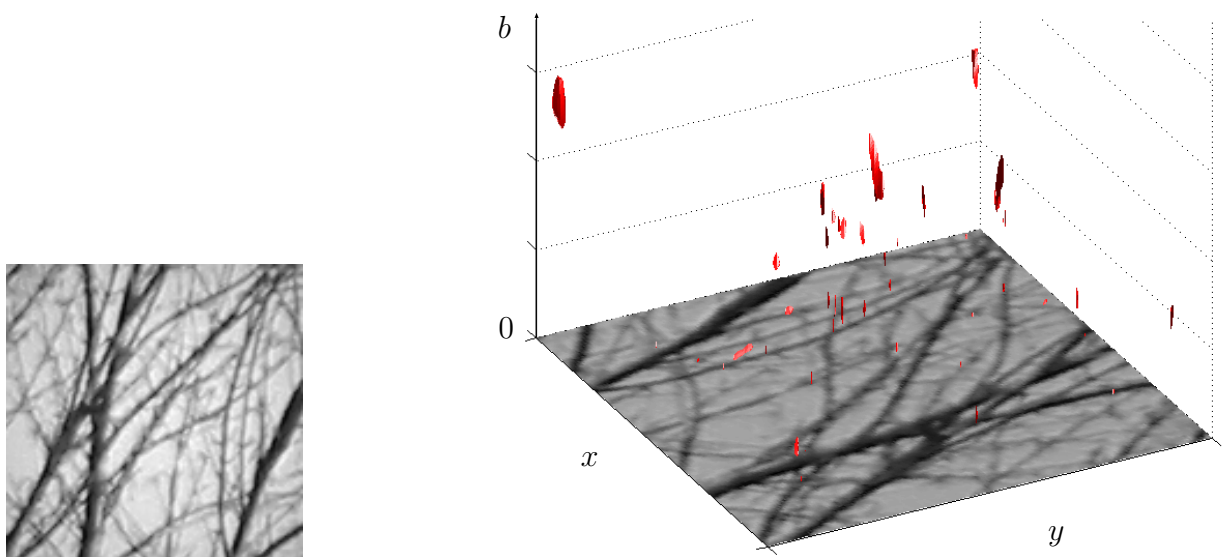

Figure 15: Zeros of tree image in monogenic scale-space. Left: original image, right: zeros (isophotes of finite, small amplitude).

obtained as the isophotes of some small constant greater than zero in order to make them

visible. Although these zero-areas can have quite large extents (see Figure 14), Theorem 4 can still be used as an approximation. In order to check the quality of the approximation, we present two experiments. In the first one, we compute the local attenuation and estimate the local phase by its Riesz transform. From the local attenuation and the estimated local phase we reconstruct the original image. Up to a DC component and a multiplicative constant, the results of the reconstruction are quite good, see Figure 16. In order to
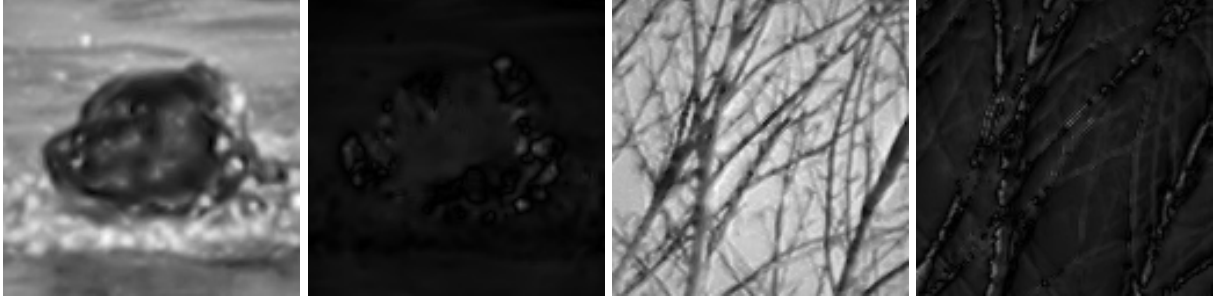

Figure 16: Reconstruction from local attenuation. From left to right: reconstruction of dog, absolute error, reconstruction of tree, absolute error.

simulate 'infinite' signals, we took a larger part of the image and multiplied it with a window function (Gaussian). The images in Figure 16 just show the center parts of the windowed images. Without a windowing function, the implicit periodicity of the images causes trouble.

Repeating the same procedure with the local phase, i.e., we try to recover the local attenuation from the local phase vector, totally fails. Basically, there are two reasons for this failure:

1. The phase vectors are wrapped, i.e., if their absolute value extends π, they are reflected in the origin, see also [15].

2. The zeros which exist in the upper halfspace affect the phase but not the attenuation. Recovering the phase from the attenuation simply suppresses the factor containing the zeros in the upper halfplane. This modified signal is still very similar to the original one. Starting from the local phase vector, however, yields instable results if zeros are present in the upper halfspace.

In general, the monogenic scale-space contains zeros in the upper halfspace even if the image is bandpass filtered beforehand. Hence, the local phase contains more information than the local amplitude, namely the information about that part of the signal which corresponds to the allpass part of a system's frequency response. This additional part of the signal does not have too much influence on the appearance of the image, see the reconstructions in Figure 16. In detail, however, there are important differences as we will show in the subsequent section.

In [15] we have stressed the fact that local amplitude and local phase are independent information. This statement must be restated in an exacter way in the current context: local amplitude and local phase are *pointwise* independent. In a local context, local attenuation and local phase vector are (approximately) related by the Riesz transform. This result is quite important for the development and comparison of special purpose filters. An example for this is given in the subsequent section.

3.4 The Relationship between Phase-Based and Amplitude-Based Image Processing

The theorems and observations from the previous sections enable us to relate phase-based image processing approaches to amplitude-based approaches on a theoretic level. For this purpose, the amplitude and the phase are extracted from the monogenic scale-space representation of the original image. In order to obtain exact results, we also have to assume that there are no zeros in the monogenic scale-space for $b > 0$. We will relax this condition later on.

Under the mentioned assumptions (the image is i1D and the monogenic scale-space contains no zeros), the local attenuation and the local phase vector form themselves a monogenic function for $b > 0$. Accordingly, we can apply (16) and (17) to relate the first derivatives of the local attenuation and those of the local phase vector:

$$\nabla_2 \cdot \mathbf{r}(\mathbf{x}; b) + \partial_b a(\mathbf{x}; b) = 0 \tag{23}$$

$$\partial_b \mathbf{r}(\mathbf{x}; b) - \nabla_2 a(\mathbf{x}; b) = 0 \; . \tag{24}$$

Furthermore, (15) implies that the phase vector field is irrotational. This is trivially fulfilled if the original image is an i1D signal, but (15) can also be considered as a criterion for the validity of (23) and (24).

Besides the first derivatives, all higher order derivatives can be computed, but since each component of a potential field is harmonic [13], the higher order derivatives do not contain new relationships.

Both equations (23) and (24) contain quite fundamental terms: the (isotropic) local frequency $\nabla_2 \cdot \mathbf{r}(\mathbf{x}; b)$ and the differential phase congruency $\partial_b \mathbf{r}(\mathbf{x}; b)$. In the case of i1D signals, i.e., the phase vector field is irrotational, the isotropic local frequency is identical to the local frequency in the main orientation, see [12]. According to [24], the local frequency can be computed directly from a quadrature filter response and its spatial partial derivatives. Adapting this idea to the 2D case, we obtain [12]

$$\nabla_2 \cdot \mathbf{r}(\mathbf{x}; b) = \frac{u(\mathbf{x}; b)(\nabla_2 \cdot \mathbf{v}(\mathbf{x}; b)) - \mathbf{v}(\mathbf{x}; b) \cdot (\nabla_2 u(\mathbf{x}; b))}{u(\mathbf{x}; b)^2 + |\mathbf{v}(\mathbf{x}; b)|^2} \; . \tag{25}$$

By means of (16) and (17) we replace the spatial derivatives with a scale derivative:

$$\nabla_2 \cdot \mathbf{r}(\mathbf{x}; b) = -\frac{u(\mathbf{x}; b)(\partial_b u(\mathbf{x}; b)) + \mathbf{v}(\mathbf{x}; b) \cdot (\partial_b \mathbf{v}(\mathbf{x}; b))}{u(\mathbf{x}; b)^2 + |\mathbf{v}(\mathbf{x}; b)|^2} \; .$$

On the other hand, by (23) we have

$$\nabla_2 \cdot \mathbf{r}(\mathbf{x}; b) = -\partial_b a(\mathbf{x}; b) = -\frac{1}{2}\partial_b \log(u(\mathbf{x}; b)^2 + |\mathbf{v}(\mathbf{x}; b)|^2)$$

which is consistent with the equation above. Hence, the local frequency is equivalent to the scale-derivative of the local attenuation. To some extent, this result is similar to the estimation of the isotropic local frequency by the quotient of two log-normal bandpass filters (see e.g. [24]), where the latter can be considered as a finite difference of frequency components at two different scales. Thus, (23) allows to switch from a finite difference in scale to a differential operator in scale, like we did in Section 3.1 with the phase congruency.

The phase congruency however, can also be computed by means of partial derivatives of the attenuation. Equation (24) implies that the differential phase congruency is given by the gradient of the attenuation. Again, we verify this result by some elementary calculations:

$$\nabla_2 a(\mathbf{x}; b) = \frac{1}{2}\nabla_2 \log(u(\mathbf{x}; b)^2 + |\mathbf{v}(\mathbf{x}; b)|^2) = \frac{u(\mathbf{x}; b)(\nabla_2 u(\mathbf{x}; b)) + \mathbf{v}(\mathbf{x}; b)(\nabla_2 \cdot \mathbf{v}(\mathbf{x}; b))}{u(\mathbf{x}; b)^2 + |\mathbf{v}(\mathbf{x}; b)|^2}$$

plugging in (17) and (16) yields (21). Hence, points of phase congruency are identical to points of vanishing gradient of the attenuation. One class of points where the gradient of the attenuation vanishes are parabolic points, i.e., points on a positive or negative ridge. Since the logarithm is strictly monotonic, these points are also points on a positive or negative ridge of the local amplitude. In other words: edge detection by means of local amplitude maxima is equivalent to edge detection by phase congruency if the Laplacian of the phase is negative.[10] This result is just contrary to looking at phase based and amplitude based approaches as being two alternative approaches (see e.g. [26]).

In order to solve this contradiction wrt. established opinions, we concentrate on an assumption made in the beginning: What happens if the image is not an i1D signal? What happens if there are zeros in the monogenic scale-space? We cannot give an exhaustive answer in this paper, the behavior of phase and attenuation at i2D points is still work in progress. However, we present a simple example of a synthetic orthogonal corner, which shows that the phase congruency is superior to the detection of local amplitude maxima. In Figure 17 the two components of the scale derivative of the phase are represented as mesh-plots. The original image can be found in the zero plane. Obviously, the zero-crossings are quite well located. In particular, at the corner the zero-crossings do not blur the contour. The gradient of the attenuation (see Figure 18) looks quite similar to the phase congruency. However, the zero-crossings are less accurately located near the corner. Hence, the main difference between approaches using the detection of local amplitude maxima and phase congruency approaches is the behavior at i2D points. This can also be verified in various edge-detection experiments in [13], where the amplitude based approaches blur the contour at corners and junctions.

---

[10]In the algorithm of Section 3.1 we replaced the evaluation of the Laplacian with a threshold on the steepness of the zero-crossing to prevent local minima.
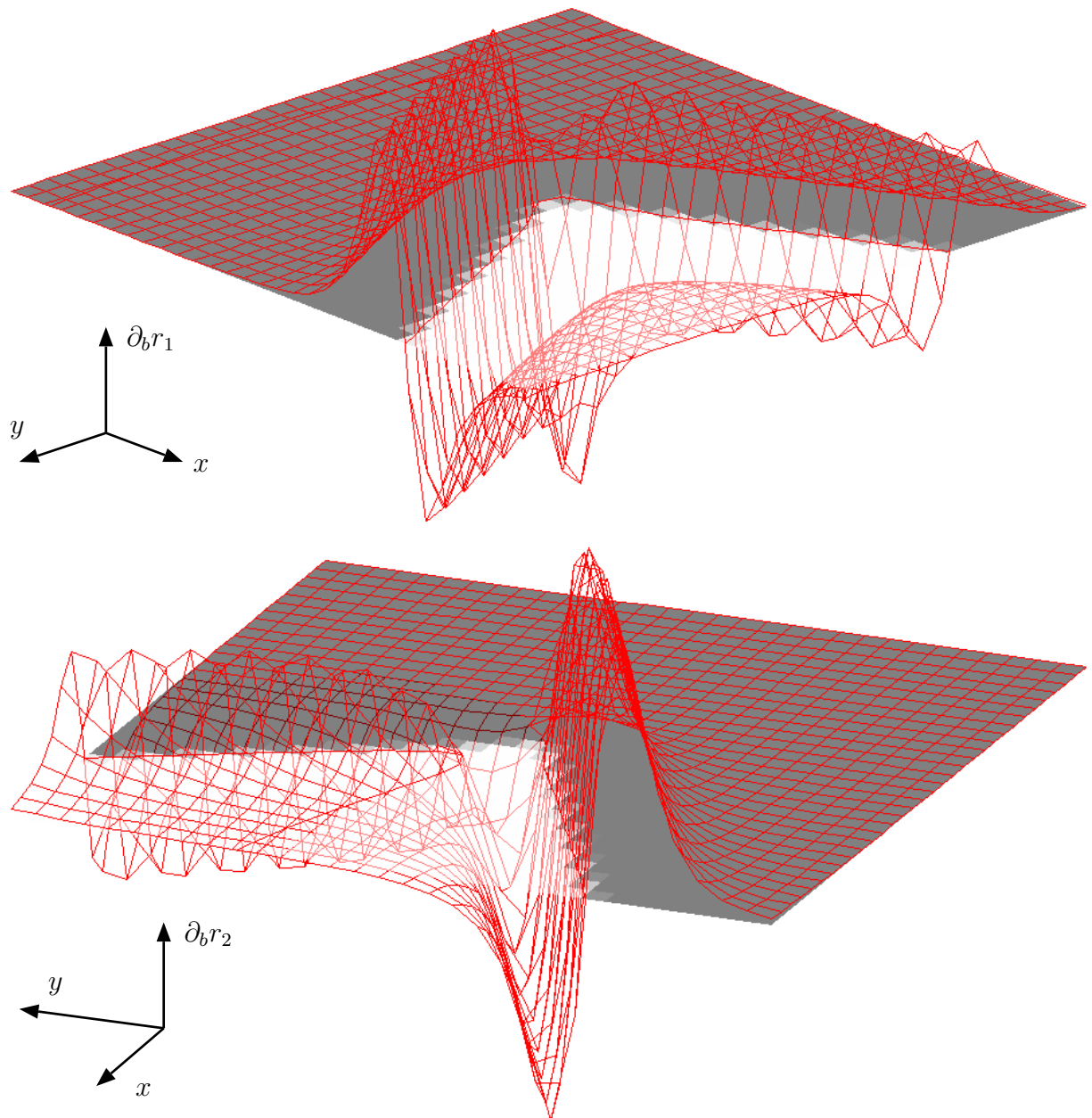
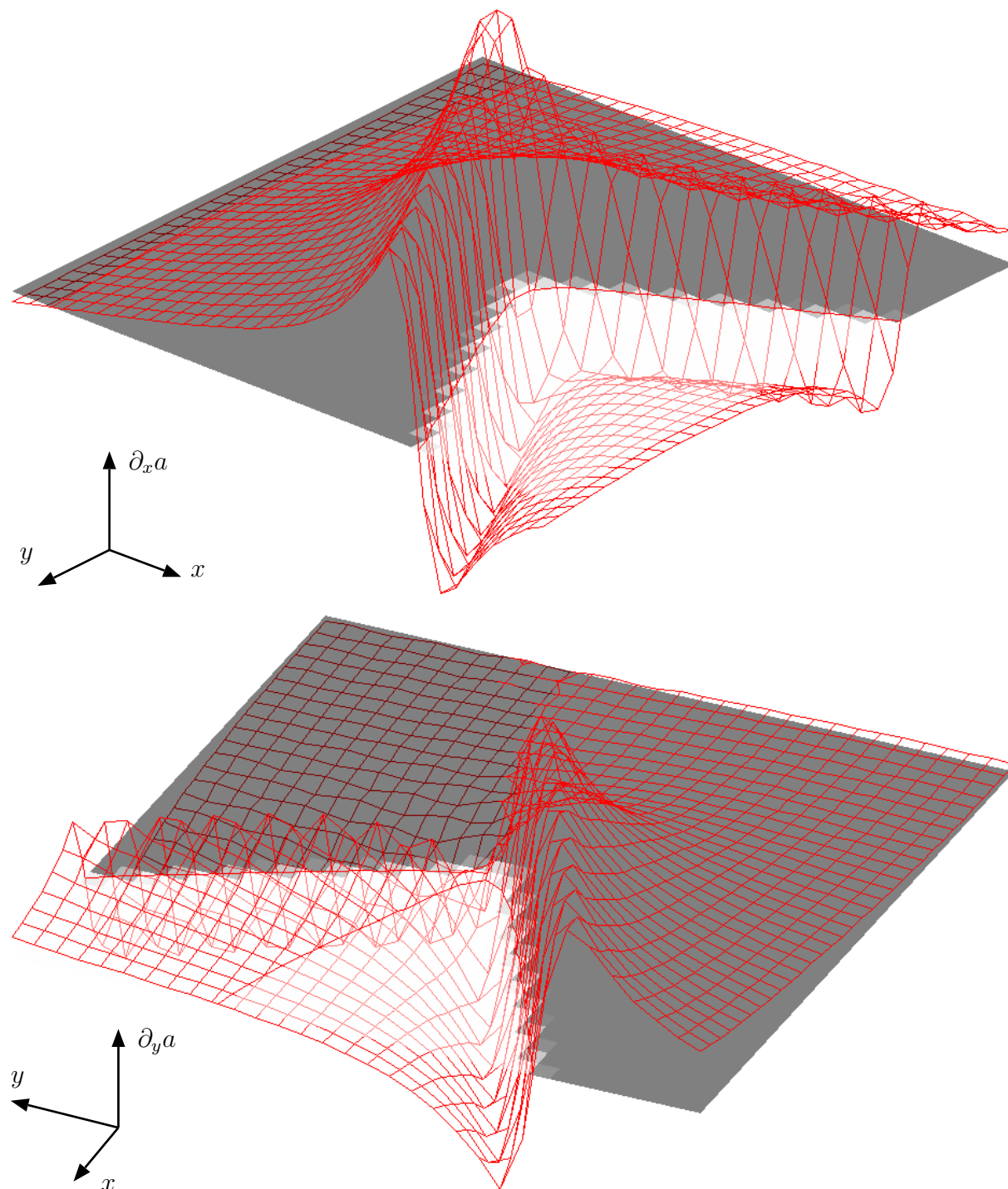Figure 17: The two components measuring the phase congruency at a corner.

Figure 18: The two partial derivatives of the local attenuation at a corner.

4   Conclusion

In this paper we have presented a unified approach to scale-space theory and phase-based image processing. The common root of the Poisson scale-space and the monogenic signal is the Laplace equation. The resulting theoretic framework yields several powerful relationships which can be exploited for image processing. However, the structure of the monogenic scale-space representation still needs further investigation to be completely understood.

Acknowledgments

Appendix

Why is Iijimas Original Uniqueness Proof Wrong?

Iijima assumes in [22], page 373, that the first n derivatives of the frequency response of the scale-space kernel do exist in the origin (equation (3.10)). In the axioms, however, no constraints are put on the frequency response (it is not even assumed that the observation transformation is connected to a frequency response at all). Replacing the derivatives in the origin with left-sided and right-sided limits, i.e., allowing a singularity in the origin, splits the inverse Fourier transform in (3.13) into two addends (using the original notation):

$$\phi(u) = \frac{1}{2\pi} \left(\int_{-\infty}^{0} \exp \left(\lim_{\tau \uparrow 0} \Psi^{(n)}(\tau) \frac{\xi^n}{n!} + i\xi u \right) d\xi + \int_{0}^{\infty} \exp \left(\lim_{\tau \downarrow 0} \Psi^{(n)}(\tau) \frac{\xi^n}{n!} + i\xi u \right) d\xi \right) .$$

This sum of integrals does not only exist for $n = 2m$ (m an integer) as stated in the original proof. In particular, the Poisson kernel ($n = 1$) is also a solution which can easily be verified.

   Changing the proof as indicated above results in just two solutions for linear scale-space kernels ($n = 1$ and $n = 2$). The remaining solutions according to [33, 10] ($K_t(u) = \exp(-2\pi|u|^\alpha t,\ \alpha \in (0, 2])$) cannot be obtained by a proof similar to the one by Iijima, since he uses explicitly the inverse Fourier transform which does only exist for certain values of α [33]. We suppose, that the Gaussian scale-space and the Poisson scale-space are the only two solutions to the Iijima axiomatic which preserve positivity and can be represented as a convolution kernel.

Convolution of two Anisotropic Poisson Kernels

Instead of considering the convolution of two anisotropic Poisson kernels, we evaluate the product of two Poisson frequency responses:

$$P(\mathbf{L}_1^{-1}\boldsymbol{\xi}; b) P(\mathbf{L}_2^{-1}\boldsymbol{\xi}; b) = \exp \left(-2\pi \sqrt{\lambda_1^{-2}u^2 + \lambda_1^2 v^2}\, b \right) \exp \left(-2\pi \sqrt{\lambda_2^{-2}u^2 + \lambda_2^2 v^2}\, b \right)$$

$$= \exp \left(-2\pi \left(\sqrt{\lambda_1^{-2}u^2 + \lambda_1^2 v^2} + \sqrt{\lambda_2^{-2}u^2 + \lambda_2^2 v^2} \right) b \right) .$$

The semigroup property implies that

$$\sqrt{\lambda_1^{-2}u^2 + \lambda_1^2 v^2} + \sqrt{\lambda_2^{-2}u^2 + \lambda_2^2 v^2} = \sqrt{\lambda_3^2 u^2 + \lambda_4^2 v^2} .$$

Squaring the latter expression yields that

$$\sqrt{\lambda_1^{-2}u^2 + \lambda_1^2 v^2}\sqrt{\lambda_2^{-2}u^2 + \lambda_2^2 v^2} = \sqrt{\lambda_1^{-2}\lambda_2^{-2}u^4 + (\lambda_1^{-2}\lambda_2^2 + \lambda_1^2\lambda_2^{-2})u^2 v^2 + \lambda_1^2\lambda_2^2 v^4}$$

has to be expressed as some linear combination of u^2 and v^2, i.e., $(\lambda_1^{-2}\lambda_2^2 + \lambda_1^2\lambda_2^{-2}) = 2$. This implies that $\lambda_1^2 - \lambda_2^2 = 0$ and due to $\lambda_1, \lambda2 > 0$ we obtain $\lambda_1 = \lambda_2$ which contradicts the original assumption $\mathbf{L}_1 \neq \mathbf{L}_2$.

Uncertainty of the 2D Poisson Kernel

The spread in the spatial domain reads (see [13])

$$
\begin{aligned}
\Delta \mathbf{x} = \sqrt{\sigma_{\mathbf{x}}^2} &= \left(\frac{\iint \mathbf{x}^2 p(\mathbf{x}; b)^2 \, dx \, dy}{\iint p(\mathbf{x}; b)^2 \, dx \, dy} \right)^{1/2} \\
&= \left(\frac{\iint \frac{\mathbf{x}^2}{(\mathbf{x}^2 + b^2)^3} \, dx \, dy}{\iint \frac{1}{(\mathbf{x}^2 + b^2)^3} \, dx \, dy} \right)^{1/2} \\
&\quad \text{change to polar coordinates } r = |\mathbf{x}|: \\
&= \left(\frac{2\pi \int_0^\infty \frac{r^3}{(r^2 + b^2)^3} \, dr}{2\pi \int_0^\infty \frac{r}{(r^2 + b^2)^3} \, dr} \right)^{1/2} \\
&= \left(\frac{\frac{1}{2b^2} - \frac{b^2}{4b^4}}{\frac{1}{4b^4}} \right)^{1/2} \\
&= b
\end{aligned}
$$

where the integrals are evaluated according to [5] 19.5.1.3 integral 63 and 71. The spread in the frequency domain is obtained as

$$
\begin{aligned}
\Delta \boldsymbol{\xi} = \sqrt{\sigma_{\boldsymbol{\xi}}^2} &= \left(\frac{\iint \boldsymbol{\xi}^2 P(\boldsymbol{\xi}; b)^2 \, du \, dv}{\iint P(\boldsymbol{\xi}; b)^2 \, du \, dv} \right)^{1/2} \\
&= \left(\frac{\iint \boldsymbol{\xi}^2 \exp(-4\pi |\boldsymbol{\xi}| b) \, du \, dv}{\iint \exp(-4\pi |\boldsymbol{\xi}| b) \, du \, dv} \right)^{1/2} \\
&\quad \text{change to polar coordinates } q = |\boldsymbol{\xi}|: \\
&= \left(\frac{2\pi \int_0^\infty q^3 \exp(-4\pi q b) \, dq}{2\pi \int_o^\infty q \exp(-4\pi q b) \, dq} \right)^{1/2} \\
&= \left(\frac{\frac{6}{(4\pi b)^4}}{\frac{1}{(4\pi b)^2}} \right)^{1/2} \\
&= \frac{\sqrt{6}}{4\pi b}
\end{aligned}
$$

where the integrals are evaluated according to [5] 19.6.1 integral 1. Hence $(\Delta \mathbf{x})(\Delta \boldsymbol{\xi}) = \frac{\sqrt{6}}{4\pi}$ in the case of the Poisson kernel which means that the uncertainty is slightly worse than for the 2D Gaussian kernel (factor $\sqrt{1.5}$).

References

[1] BABAUD, J., WITKIN, A. P., BAUDIN, M., AND DUDA, R. O. Uniqueness of the gaussian kernel for scale-space filtering. *IEEE Transactions on Pattern Analysis and Machine Intelligence 8*, 1 (1986), 26–33.

[2] BRACEWELL, R. N. *The Fourier transform and its applications.* McGraw Hill, 1986.

[3] BRACEWELL, R. N. *Two-Dimensional Imaging.* Prentice Hall Signal Processing Series. Prentice Hall, Englewood Cliffs, 1995.

[4] BRACKX, F., DELANGHE, R., AND SOMMEN, F. *Clifford Analysis.* Pitman, Boston, 1982.

[5] BRONSTEIN, I., SEMENDJAJEW, K., MUSIOL, G., AND MÜHLIG, H. *Taschenbuch der Mathematik.* Verlag Harri Deutsch, Frankfurt, 1993.

[6] BURG, K., HAF, H., AND WILLE, F. *Höhere Mathematik für Ingenieure, Band V Funktionalanalysis und Partielle Differentialgleichungen.* Teubner Stuttgart, 1993.

[7] BURT, P. J., AND ADELSON, E. H. The Laplacian pyramid as a compact image code. *IEEE Trans. Communications 31*, 4 (1983), 532–540.

[8] CATTÉ, F., LIONS, P.-L., MOREL, J.-M., AND COLL, T. Image selective smoothing and edge detection by nonlinear diffusion. *SIAM J. Numer. Analysis 32* (1992), 1895–1909.

[9] DUITS, R., FLORACK, L. M. J., DE GRAAF, J., AND TER HAAR ROMENY, B. M. On the axioms of scale space theory. *Journal of Mathematical Imaging and Vision* (2002). submitted.

[10] DUITS, R., FLORACK, L. M. J., DE GRAAF, J., AND TER HAAR ROMENY, B. M. Scale space axioms critically revisited. In *Signal and Image Processing (SIP)* (2002). to appear.

[11] EVANS, M., HASTINGS, N., AND PEACOCK, J. B. *Statistical Distributions*, 3rd. ed. Wiley-Interscience, 2000.

[12] FELSBERG, M. Disparity from monogenic phase. In *24. DAGM Symposium Mustererkennung, Zürich* (2002), L. v. Gool, Ed., Lecture Notes in Computer Science, Springer-Verlag, Heidelberg. to appear.

[13] FELSBERG, M. *Low-Level Image Processing with the Structure Multivector.* PhD thesis, Institute of Computer Science and Applied Mathematics, Christian-Albrechts-University of Kiel, 2002. TR no. 0203, available at `http://www.informatik.uni-kiel.de/reports/2002/0203.html`.

[14] FELSBERG, M., AND SOMMER, G. A new extension of linear signal processing for estimating local properties and detecting features. In *22. DAGM Symposium Mustererkennung, Kiel* (2000), G. Sommer, N. Krüger, and C. Perwass, Eds., Springer-Verlag, Heidelberg, pp. 195–202.

[15] FELSBERG, M., AND SOMMER, G. The monogenic signal. *IEEE Transactions on Signal Processing 49*, 12 (December 2001), 3136–3144.

[16] FELSBERG, M., AND SOMMER, G. Scale adaptive filtering derived from the Laplace equation. In *23. DAGM Symposium Mustererkennung, München* (2001), B. Radig and S. Florczyk, Eds., vol. 2191 of *Lecture Notes in Computer Science*, Springer-Verlag, Heidelberg, pp. 124–131.

[17] FELSBERG, M., AND SOMMER, G. The structure multivector. In *Applied Geometrical Algebras in Computer Science and Engineering* (2002), Birkhäuser, Boston, pp. 437–448.

[18] GRANLUND, G. H. In search of a general picture processing operator. *Computer Graphics and Image Processing 8* (1978), 155–173.

[19] GRANLUND, G. H., AND KNUTSSON, H. *Signal Processing for Computer Vision.* Kluwer Academic Publishers, Dordrecht, 1995.

[20] HUMMEL, R. A. Representations based on zero-crossings in scale space. In *Proc. IEEE Comp. Soc. Conf. Computer Vision and Pattern Recognition* (Miami Beach, 1986), pp. 204–209.

[21] HURT, N. E. *Phase Retrieval and Zero Crossings.* Kluwer Academic, Dordrecht, 1989.

[22] IIJIMA, T. Basic theory of pattern observation. In *Papers of Technical Group on Automata and Automatic Control, IECE, Japan* (December 1959).

[23] IIJIMA, T. Observation theory of two-dimensional visual patterns. In *Papers of Technical Group on Automata and Automatic Control, IECE, Japan* (October 1962).

[24] JÄHNE, B. *Digitale Bildverarbeitung.* Springer-Verlag, Berlin, 1997.

[25] KOENDERINK, J. J. The structure of images. *Biological Cybernetics 50* (1984), 363–370.

[26] KOVESI, P. Image features from phase information. *Videre: Journal of Computer Vision Research 1*, 3 (1999).

[27] KRANTZ, S. G. *Handbook of Complex Variables.* Birkhäuser, Boston, 1999.

[28] KRIEGER, G., AND ZETZSCHE, C. Nonlinear image operators for the evaluation of local intrinsic dimensionality. *IEEE Transactions on Image Processing 5*, 6 (June 1996), 1026–1041.

[29] LINDEBERG, T. *Scale-Space Theory in Computer Vision*. The Kluwer International Series in Engineering and Computer Science. Kluwer Academic Publishers, Boston, 1994.

[30] LINDEBERG, T. *On the axiomatic foundations of linear scale-space: Combining semi-group structure with causality vs. scale invariance*. Kluwer Academic, 1997, ch. 6.

[31] PAPOULIS, A. *The Fourier Integral and its Applications*. McGraw-Hill, New York, 1962.

[32] PAPOULIS, A. *Probability, Random Variables and Stochastic Processes*. McGraw-Hill, 1965.

[33] PAUWELS, E. J., VAN GOOL, L. J., FIDDELAERS, P., AND MOONS, T. An extended class of scale-invariant and recursive scale space filters. *IEEE Transactions on Pattern Analysis and Machine Intelligence 17*, 7 (July 1995), 691–701.

[34] PERONA, P., AND MALIK, J. Scale-space and edge detection using anisotropic diffusion. *IEEE Trans. Pattern Analysis and Machine Intelligence 12*, 7 (1990), 629–639.

[35] REISFELD, D. The Constrained Phase Congruency feature detector: Simultaneous localization, classification and scale determination. *Pattern Recognition Letters 17* (1996), 1161–1169.

[36] SCHIFF, J. L. *The Laplace Transform*. Undergraduate Texts in Mathematics. Springer-Verlag, New York, 1999.

[37] SOCHEN, N., KIMMEL, R., AND MALLADI, R. A geometrical framework for low level vision. *IEEE Trans. on Image Processing, Special Issue on PDE based Image Processing 7*, 3 (1998), 310–318.

[38] STEIN, E., AND WEISS, G. *Introduction to Fourier Analysis on Euclidean Spaces*. Princeton University Press, New Jersey, 1971.

[39] WEICKERT, J. *Anisotropic Diffusion in Image Processing*. PhD thesis, Faculty of Mathematics, University of Kaiserslautern, 1996.

[40] WEICKERT, J. A review of nonlinear diffusion filtering. In *Scale-Space Theory in Computer Vision* (1997), B. ter Haar Romeny, L. Florack, J. Koenderink, and M. Viergever, Eds., vol. 1252 of *LNCS*, Springer, Berlin, pp. 260–271.

[41] WEICKERT, J., ISHIKAWA, S., AND IMIYA, A. Scale-space has first been proposed in Japan. *Mathematical Imaging and Vision 10* (1999), 237–252.